Systems/Circuits

HippoBellum: Acute Cerebellar Modulation Alters Hippocampal Dynamics and Function

Zachary Zeidler,[1] Katerina Hoffmann,[2] and Esther Krook-Magnuson[2]
[1]Graduate Program in Neuroscience, University of Minnesota, Minneapolis, Minnesota 55455, and [2]Department of Neuroscience, University of Minnesota, Minneapolis, Minnesota 55455

Here we examine what effects acute manipulation of the cerebellum, a canonically motor structure, can have on the hippocampus, a canonically cognitive structure. In male and female mice, acute perturbation of the cerebellar vermis (lobule 4/5) or simplex produced reliable and specific effects in hippocampal function at cellular, population, and behavioral levels, including evoked local field potentials, increased hippocampal cFos expression, and altered CA1 calcium event rate, amplitudes, and correlated activity. We additionally noted a selective deficit on an object location memory task, which requires objection-location pairing. We therefore combined cerebellar optogenetic stimulation and CA1 calcium imaging with an object-exploration task, and found that cerebellar stimulation reduced the representation of place fields near objects, and prevented a shift in representation to the novel location when an object was moved. Together, these results clearly demonstrate that acute modulation of the cerebellum alters hippocampal function, and further illustrates that the cerebellum can influence cognitive domains.

Key words: **cerebellum; hippocampus; miniscope; object memory; spatial memory**

Significance Statement

The cerebellum, a canonically motor-related structure, is being increasingly recognized for its influence on nonmotor functions and structures. The hippocampus is a brain region critical for cognitive functions, such as episodic memory and spatial navigation. To investigate how modulation of the cerebellum may impact the hippocampus, we stimulated two sites of the cerebellar cortex and examined hippocampal function at multiple levels. We found that cerebellar stimulation strongly modulates hippocampal activity, disrupts spatial memory, and alters object-location processing. Therefore, a canonically cognitive brain area, the hippocampus, is sensitive to cerebellar modulation.

Introduction

While the cerebellum is a canonically motor-related structure, it is being increasingly appreciated for its relationship to cognitive brain areas and tasks (Strick et al., 2009; King et al., 2019; Schmahmann, 2019; Argyropoulos et al., 2020). The hippocampus, in contrast, is a canonically cognitive brain region, important for navigating through time and space (O'Keefe and Nadel, 1978; Redish, 1999; Eichenbaum and Cohen, 2014; Hartley et al., 2014; Sabariego et al., 2019). The hippocampus uses a convergence of information to maintain cognitive maps (B. L. McNaughton et al., 2006; van Strien et al., 2009), including self-motion cues, and may therefore be reliant on information indirectly passed from the cerebellum (Hitier et al., 2014; Rondi-Reig et al., 2014; Leong et al., 2019). Indeed, lesions or genetic alterations affecting the cerebellum can alter spatial navigation, exploration strategies, and even place cell expression under certain conditions (Joyal et al., 1996, 2001; Petrosini et al., 1996; Hilber et al., 1998; Leggio et al., 1999, 2000; Colombel et al., 2004; Mandolesi et al., 2007; Rochefort et al., 2011; Lefort et al., 2019), suggesting an impact of the cerebellum on the hippocampus.

Received Apr. 2, 2020; revised June 14, 2020; accepted July 9, 2020.

Author contributions: Z.Z. and E.K.-M. designed research; Z.Z. and K.H. performed research; Z.Z. contributed unpublished reagents/analytic tools; Z.Z. and K.H. analyzed data; Z.Z. and E.K.-M. wrote the first draft of the paper; Z.Z., K.H., and E.K.-M. edited the paper; Z.Z. and E.K.-M. wrote the paper.

This work (and the E.K.-M. laboratory) was supported by Winston and Maxine Wallin Neuroscience Discovery Fund to E.K.-M.; National Institutes of Health Grants R00NS087110, R01NS104071, and R01NS112518 to E.K.-M.; National Institute of Neurological Disorders and Stroke 1F31NS103320 to Z.Z.; University of Minnesota MnDRIVE (Minnesota's Discovery, Research and Innovation Economy) initiative and Informatics Institute to E.K.-M. and Z.Z.; and McKnight Land-Grant Professorship to E.K.-M. GCaMP6f was developed by the GENIE Program and the Janelia Farm Research Campus, specifically Drs. Vivek Jayaraman, Rex A. Kerr, Douglas S. Kim, Loren L. Looger, and Karel Svoboda. We thank the entire E.K.-M. laboratory, especially Zachary Montes for assistance with behavioral testing, Shabad Washist for immunohistochemical processing, Chris Krook-Magnuson for development of LFP analysis software, Tom Richner for coding assistance, and Isaac Hoff for colony management; A. David Redish for discussions of place cells and experimental design; and Michael Benneyworth and the University of Minnesota Mouse Behavior Core, Mark Sanders and the University of Minnesota University Imaging Center, and Peyman Golshani and the University of California Los Angeles Miniscope project for providing open-source materials and hosting their workshop.

The authors declare no competing financial interests.

Correspondence should be addressed to Zachary Zeidler at zeidl012@umn.edu.

https://doi.org/10.1523/JNEUROSCI.0763-20.2020

The cerebellum, via the cerebellar nuclei, has broad extracerebellar projections to motor and nonmotor areas alike (Schmahmann, 1996; Strick et al., 2009). Recent anatomic tracing suggests (multisynaptic) connectivity between the cerebellum and the hippocampus (Bohne et al., 2019; Watson et al., 2019; Krook-Magnuson, 2020), and inhibition of the cerebellar cortex produces broad yet selective modulation of cortical and subcortical regions, including the hippocampus (Choe et al., 2018). We therefore asked what impact acute modulation of the cerebellum might have on hippocampal function, including processing of objects in space.

Different regions of the cerebellum may interact with the hippocampus in distinct ways. For example, hippocampal and cerebellar oscillations can show task-specific coherence, with differential encoding across cerebellar regions (Hoffmann and Berry, 2009; Wikgren et al., 2010; McAfee et al., 2019; Watson et al., 2019). Distinct yet overlapping cerebello-hippocampal interactions are also seen in a mouse model of temporal lobe epilepsy, where optogenetic manipulation of the cerebellum can inhibit hippocampal seizures (Krook-Magnuson et al., 2014). Manipulation of either the medial cerebellar cortex (vermis lobule IV/V) or more lateral cerebellar cortex (simplex lobule) is able to acutely inhibit seizures. Activation of the vermis, however, additionally produces a prolonged antiseizure effect, which is not present with activation of the simplex (Krook-Magnuson et al., 2014). We therefore addressed not only what impact acute modulation of the cerebellum might have on hippocampal function in healthy animals, but also examined two cerebellar locations in particular, the simplex and vermis (lobule IV/V), and used the same light parameters as used in the previous epilepsy studies. This allowed us to determine whether overlapping yet distinct effects of these particular cerebellar regions could also be observed in healthy animals.

While encoding of object identity (alone) is minimal in the hippocampus (Komorowski et al., 2009; Manns and Eichenbaum, 2009), CA1 neurons can be specifically sensitive to object-location pairings, and more CA1 neurons will express place fields when objects are present in an environment (Komorowski et al., 2009; Burke et al., 2011). In line with this, tasks that require object identity memory are generally insensitive to hippocampal damage (Mumby et al., 2002; Winters et al., 2004), while object-location memory is strongly hippocampal dependent (Winters and Bussey, 2005; Balderas et al., 2008; Haettig et al., 2011). We find that cerebellar stimulation, of the simplex or vermis, produces a significant deficit on an object-location memory task, but not an object-recognition task, suggesting that cerebellar manipulation may have a strong and specific impact on object-place processing and therefore possibly hippocampal function.

Confirming an effect of cerebellar stimulation on the hippocampus itself, acute cerebellar stimulation evoked robust changes to hippocampal local field potential (LFP) recordings. Notably, while similar effects were seen with vermal or simplex stimulation, vermal stimulation generally produced larger hippocampal effects. Similarly, prolonged stimulation caused distinct patterns of hippocampal cFos expression between simplex- and vermis-targeted animals, with overall greater changes following vermal targeting, including particularly strong increases in CA1. One-photon calcium imaging in awake behaving animals revealed effects on CA1 calcium transients and temporally correlated activity across a large number of cells at both the onset and offset of cerebellar modulation, particularly with activation of the vermis.

Importantly, we also observed altered object-location processing by hippocampal CA1 neurons, including in their expression of place fields. Specifically, cerebellar stimulation reduced the representation of place fields near objects, and prevented a shift in representation to the novel location when an object was moved, providing a clear potential mechanism for the observed deficits on the object location memory (OLM) task.

Together, these findings provide key insight into how cerebellar modulation impacts hippocampal function, and broadens our understanding of cerebellar influence on cognitive domains.

Materials and Methods

All experimental protocols were approved by the University of Minnesota's Institutional Animal Care and Use Committee.

Animals

Mice were bred in-house and sexed after weaning based on external genitalia. PV-Cre (B6;129P2-Pvalbtm1(cre)Arbr/J, The Jackson Laboratory, stock #008069) (Hippenmeyer et al., 2005) and Pcp-Cre (B6.Cg-Tg (Pcp2-cre)3555Jdhu/J, The Jackson Laboratory, stock #010536) (Zhang et al., 2004) were crossed with Ai32 mice (Rosa-CAG-LSL-ChR2H134R-EYFP-deltaNeo, The Jackson Laboratory, stock #012569) (Madisen et al., 2012) to create PV-ChR and Pcp-ChR mice with channelrhodopsin2 (ChR) exclusively expressed in parvalbumin (PV)- or Pcp-expressing cells, respectively. These crosses also generated non–opsin-expressing animals (Cre and/or ChR-negative), which were used as control animals. For a subset of behavior experiments, specifically initial OLM and object recognition memory (ORM) experiments, PV-ChR animals were used. All other experiments used Pcp-ChR animals.

Before implantation, animals were group housed. Following implantation, animals were individually housed to prevent damage to the implants. In both single and group housing conditions, animals received *ad libitum* access to food and water. Animals were on a 12 h light/dark cycle. Although our experiments were not specifically designed to test for sex differences, sex was examined as a *post hoc* factor and no significant differences were found on any experiments.

Surgery

All surgeries were performed stereotaxically with the animal atop a heating pad and under 1%-2% isoflurane anesthesia.

Viral injections

Pcp-ChR mice were injected with 600 nl of AAV1.Syn.GCaMP6f virus at a titer of 2.7E13 (AAV1.Syn.GCaMP6f was a gift from GENIE Project to Addgene; Addgene plasmid #100837; RRID:Addgene_100837) (Chen et al., 2013) using a Hamilton Neuros syringe (part #65459). The injection was made into CA1 of the left dorsal hippocampus: 0.2 cm posterior, 0.175 cm left, 0.15 cm ventral in coordinates relative to bregma, at an approximate rate of 100 nl per minute. After delivering the viral load, the syringe was left in place for 5 min before being retracted.

Implant surgery

For all implant surgeries, implants were secured with cyanoacrylate, a small skull screw, and dental cement.

Grin lens implantation. At least 2 weeks following AAV1.Syn.GCaMP6f transduction, a gradient refractive index (GRIN) lens was implanted slightly off-center from the injection cite (0.2 cm posterior to bregma, 0.15 cm left). A 2 mm circular craniotomy was made around the target site, and the cortex was aspirated using a blunt 27-gauge needle attached to a vacuum and continuous application of ACSF. The aspiration stopped when the fibers of the alveus were revealed. The GRIN lens (0.25 pitch, 0.55 NA, 1.8 mm diameter, 4.3 mm in length, Edmunds Optics) was lowered onto CA1 using a stereotaxic arm to a depth of 0.135 cm ventral from the skull at posterior edge of the craniotomy. The lens was covered with Kwik-Sil (World Precision Instruments), and animals received daily intraperitoneal injections of dexamethasone for 5 d. At least 2 weeks after GRIN lens implantation, a baseplate was cemented around the lens to fix the FOV of the miniscope. Following experiments, tissue was processed to ensure appropriate targeting of the GRIN lens; all animals showed appropriate targeting.

Optic fiber implantation. For delivering light to the cerebellar cortex, mice were implanted with an optical fiber (Thorlabs, FT200UMT, Ø200μm, 0.39 NA) targeting lobule IV/V (0.59 cm posterior to bregma, midline, ~0.001 cm ventral to brain surface) and/or the right simplex lobule (0.57 cm posterior to bregma, 0.22 cm right of midline, ~0.001 cm ventral to brain surface).

Estimation of tissue volume directly affected by light delivery. Given the physical properties of the implanted fibers (200 µm diameter, numerical aperture 0.39, flat cleaved tip), the average light power from the fiber tip (5.5 mW of 473 nm light), and reported values for the required irradiance for activating ChR (1 mW/mm^2) (Aravanis et al., 2007), we calculate that we reached an activation depth of 0.75 mm (https://web.stanford.edu/group/dlab/cgi-bin/graph/chart.php). This results in a cone of activation with a volume of ~0.05 mm^3.

Optrode implantation. For delivering light and recording activity from the cerebellar cortex, mice were implanted with optrodes (optical fiber and electrode) at the same coordinates as those with optical fibers. Optrodes were made in-house, combining an optical fiber with a twisted-wire bipolar electrode (Plastics One, 2-channel stainless-steel, MS303/3-A/SPC). Mice used for *in vivo* electrophysiology were additionally implanted with a twisted-wire bipolar electrode in the left dorsal hippocampus (0.26 cm posterior, 0.175 cm left, 0.14 cm ventral to bregma).

Following all implantation surgeries, animals received Motrin in their drinking water for 3 d for pain management.

cFos

To examine cFos expression following optogenetic cerebellar manipulation, opsin-expressing mice were matched to non–opsin-expressing mice and subjected to 1 h of periodic (every 60 s) blue light pulses (3 s duration, ~7 Hz, 33% duty cycle). Approximately 15 min later, the animal was anesthetized using an intraperitoneal overdose of tribromoethanol and transcardially perfused with PBS and then 4% PFA. Brains were collected and stored in 4% PFA, and later sliced coronally into 50-µm-thick sections. A 1-in-4 series was collected and subjected to *cFos* immunohistochemistry. Sections were washed and blocked with 5% BSA for 1 h before overnight incubation in 1:1000 dilution of rabbit anti-cFos (Cell Signaling Technology, #2250). The following day, a 1:2000 dilution of donkey anti-rabbit AlexaFluor-594 was applied for 2 h and washed. Sections were then mounted with Vectashield mounting media with DAPI.

Sections were visualized using an epifluorescent microscope (Leica Microsystems, DM2500). Using a 10× objective, a series of overlapping images from the left hippocampus were collected to stitch together a single composite image (Image Composite Editor, Microsoft). Using stitched images, a custom script in Fiji (Schindelin et al., 2012) was run to automatically quantify immunopositive cells within manually drawn ROIs. ROIs were drawn around each lamina and layer of the hippocampus proper and dentate gyrus. CA2 was excluded from analysis because of high background labeling. Counts in suprapyramidal laminae (alveus, stratum oriens) were combined, as were counts in infrapyramidal laminae (stratum radiatum, stratum lacunosum moleculare, and in CA3, stratum lucidum). Counts for a given region were tallied and summed across all hippocampal sections to create one value for each ROI.

In vivo electrophysiology

Electrical patch cables were connected to the hippocampal and cerebellar electrode pedestals, and an optical patch cable to the cerebellar optical fiber. The wideband LFP signal (differential of the two twisted wires) was recorded at 1000 Hz and amplified 5000-10,000 times (Brownlee Precision 410, Neurophase). A series of blue light pulses from LEDs (Plexon) or lasers (Shanghai Laser & Optics Century) was delivered to the cerebellum at 30 s intervals (3 s durations, 10 ms on periods, and a range of frequencies between 1 and 50 Hz; or 3 s of 50 ms on, 100 ms off light pulses, mimicking light delivery used during all other experiments).

In vivo electrophysiological recordings were analyzed with custom MATLAB scripts and the Chronux version 2.12 toolbox (Mitra and Bokil, 2008) for each animal and light frequency. Recordings were aligned to the onset of the light stimulus. Sections likely containing strong movement artifact (defined as a signal range greater than twice the average range for that animal) were removed and excluded from analysis. A 60 Hz bandstop filter was applied to all analyses.

To quantify the change in recording power at the stimulation frequency for each light stimulus, a bandpass filter was applied with a 1 Hz band centered on the stimulation frequency, and the bandpower calculated. This was done over the 3 s before light delivery and the 3 s during light delivery. These values were averaged across all trials for that stimulation frequency, and the power during light expressed as a percent increase from the period before light, using custom MATAB-based scripts (Christenson Wick et al., 2019) (available at https://github.com/KM-Lab/SpectrumAndCoherence).

The same custom scripts were used to generate differential spectrograms (Extended Data Fig. 2-1, 2-2, 2-3, 2-4, 2-5). Trial-averaged moving time spectrograms were generated for each animal and light frequency for 3 s before light delivery. The moving window had a size of 1 s and a step size of 100 ms. The resulting power per frequency bin was then averaged over the 3 s prior period. This generated baseline values. These baseline values were used to calculate the percent increase in power during and after light delivery (using the same window and step size in trial-averaged moving time spectrogram construction). The subsequent spectrograms were then averaged across genotype and recording location.

Behavior

In PV-ChR animals, OLM and ORM were conducted using published protocols, including the objects of investigation (Ciernia and Wood, 2014; Zeidler et al., 2018; Kim et al., 2020). Briefly, animals were handled for 90 s each day for 5 d. Then, they were habituated to the testing arena for 5 min, twice a day, for 3 d. After habituation, objects were introduced to the arena on subsequent days. The first object day (training day) featured two identical objects placed in the arena during which the animal was allowed to freely explore for 10 min. The following day (testing day), a novelty was introduced. For the OLM, the same two objects were returned to the arena, but one of the objects was moved to a novel location. For the ORM, two objects were put back into the same location, but one of the objects was novel. The session on the testing day lasted for 5 min.

During both the training and testing days, a blue light stimulus (3 s duration, ~7 Hz, 33% duty cycle) was delivered once a minute. Videos of the training and testing sessions were recorded and scored offline by a reviewer blinded to experimental group. Between each subject, the arena and objects were wiped with 70% ethanol. The testing order was balanced between subjects, as was the side of the arena that the spatial novelty was introduced, and the identity of the novel object.

The OLM arena was rectangular (43 L × 22 W × 20 H cm), black with a white vertical stripe up one side. The ORM arena was circular (30 cm diameter; 26 cm height), white with a black vertical stripe up one side. A thin layer of bedding material covered the ORM arena floor. In Pcp-ChR animals, the OLM and ORM tests were conducted in largely the same manner, but with an abbreviated handling and habituation phase (Christenson Wick et al., 2019).

To quantify the behavior, a discrimination index (DI) was calculated: time investigating the novel object minus the time investigating the familiar object divided by the combined time investigating both objects, multiplied by 100. Investigation was defined as by Ciernia and Wood (2014): briefly, active orientation of the subject's nose toward and within 1 cm of the object, exclusive of non–object-oriented-investigatory behaviors (including digging near the object, sitting atop the object, and peering above the object). Analysis was performed by experimenters blinded to the experimental condition. A criterion of 3 s total exploration time was predetermined and used to exclude inactive subjects. An additional criterion of a $-20 > \mathrm{DI} < 20$ was applied to the training phase, to exclude subjects exhibiting a bias toward a specific object or side of the arena (ORM exclusions: 3 vermis-positive, 3 vermis-negative, 2 simplex-positive, 1 simplex-negative, 2 hippocampus-positive, 4 hippocampus-negative; OLM exclusions: 7 vermis-positive, 5 vermis-negative, 6 simplex-positive, 5 simplex-negative, 5 hippocampus-positive, 8 hippocampus-negative).

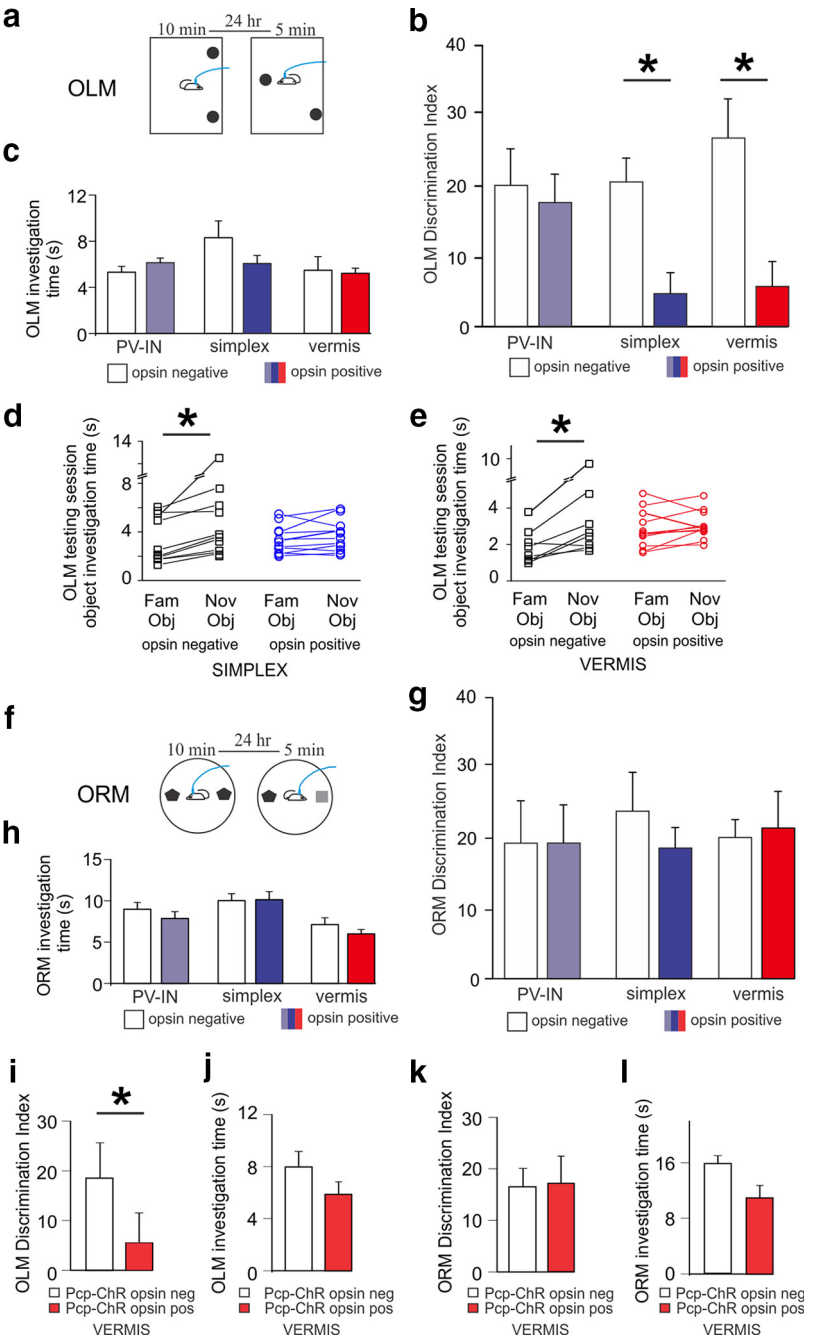

Figure 1. Optogenetic excitation of the cerebellar cortex disrupts performance specifically on a spatial memory task. ***a***, Schematic of OLM task. ***b***, DI of novel object location. Cerebellar stimulated animals showed impaired novel object-location discrimination. $*p < 0.05$ (Mann–Whitney). ***c***, Total time spent investigating objects during the testing day on the OLM task. Overall investigation was similar between opsin-negatives and -positives. ***d***, Time spent investigating individual objects during OLM testing session in simplex-targeted animals. Opsin-negatives spent significantly more time investigating the novel (moved) object, whereas opsin-positive simplex-targeted animals did not. $*p < 0.05$ (paired *t* test). ***e***, Same as in ***d***, but for vermis targeted. ***f-h***, Same as in ***a-c***, but for ORM task. No difference between groups was observed for ORM discrimination of novel object identity nor investigation time. ***i-l***, Results from an additional cohort of vermis-targeted Pcp-ChR animals replicating the (***i***) impaired OLM DI with no reduction in (***j***) OLM investigation time, (***k***) ORM DI, or (***l***) ORM investigation time. $*p < 0.05$ (Mann–Whitney). PV-IN, Stimulation of hippocampal PV-expressing interneurons. No effect was seen on OLM or ORM when stimulating hippocampal PV-INs, matching previous reports.

Miniscope imaging acquisition, analysis, and object exploration experiments

Calcium imaging data were acquired via a microendoscope (version 3.2 Miniscope) assembled in-house (Cai et al., 2016) (custom CMOS Imaging Sensory PCB, Sierra Circuits; excitation blue LED, Digikey; for complete details and parts list, see publication and online repository at www.miniscope.org). The Miniscope featured a 700 μm × 450 μm FOV with a resolution of ~1 μm per pixel. Calcium videos were acquired at 20 frames per second. Videos of mouse behavior were acquired with a webcam at 30 frames per second (Logitech c270) and aligned offline to the Miniscope.

Object exploration experiment with hippocampal calcium imaging

Before any behavioral testing with the Miniscope, animals were handled daily for 2 min on 3 consecutive days, then habituated to wearing the miniscope and optic patch cable in an open-field for 10 min a day for 3 consecutive days.

For the object exploration experiment, a white circular arena (50 cm diameter × 20 cm height) was used and decorated along the walls with distinct patterns and shapes in each cardinal direction. Two identical objects were placed off-center on one side of the arena. The subject was connected to a patch cable and Miniscope, then placed into a holding cage for 5 min, after which, the animal was placed into the arena and allowed to explore for 12 min. During that time, blue light was delivered to the animal in the same fashion as described in the OLM experiment (3 s duration, ~7 Hz, 33% duty cycle, every 60 s). Then the animal was returned to its home cage and the arena cleaned with 70% ethanol. The following day, the same protocol was followed, except 1 of the objects (balanced between subjects) was moved to the center of the opposite side of the arena. One week later, the protocol was repeated, targeting the patch cable to the other cerebellar optic fiber and using a different set of objects in different starting locations. The starting fiber location was counterbalanced between subjects.

Calcium video processing

Calcium imaging videos were processed using the MIN1PIPE calcium imaging signal extraction pipeline (Lu et al., 2018), which combines modules for background removal (Perona and Malik, 1990; Serra and Vincent, 1992), movement correction (Lucas and Kanade, 1981; Shi and Tomasi, 1994; Vercauteren et al., 2009), and automatic ROI identification and signal extraction based on spatial (i.e., location) and temporal (i.e., fluorescent changes) properties of individual units (Hochreiter and Schmidhuber, 1997; LeCun et al., 2015; Pnevmatikakis et al., 2016). *A priori* structural element estimates were initialized at 5 pixels to seed ROI detection. On average, 144 ROIs were detected in a recording. From the resulting calcium transients, fast non-negative deconvolution (Zhou et al., 2018) was used for specific analyses to deconvolve the fluorescent changes of each neuron into approximations of the underlying neural activity. Animal position was tracked using ezTrack (Pennington et al., 2019).

Calcium event rate and correlated activity analysis

Calcium signals were aligned to stimulus onset and analyzed for changes in fluorescence, event rate, and correlated activity. Deconvolved calcium

transients (Pnevmatikakis et al., 2016) were used to examine event amplitude. For event rate analysis, deconvolved event data with zero amplitude remained at 0, and all other time points were set to 1. For each stimulus, activity was baseline adjusted to visualize changes. The data were then smoothed using a 5 frame (0.25 s) moving average window over prestimulus, during stimulus, and poststimulus time bins.

For correlated activity analysis, activity was binned into 100 ms sections. For each stimulus, a correlation matrix over a 1 s sliding window (100 ms step size) was then generated for periods before, during, and after the light stimulus for each light delivery. The mean of the absolute values of the correlation matrix was taken and used as the population correlation measure for that light stimulus. For each stimulus, the correlation coefficients were baseline-adjusted to visualize change in population correlation coefficients.

Place cell analysis

The location of the animal was binned into 2.5 cm square bins. All data were speed filtered using an instantaneous speed threshold of 2.5 cm/s, then smoothed using a Gaussian kernel (σ = 2.5 cm). Deconvolved calcium events (i.e., approximations of neural activity) were summed in each spatial bin and then smoothed using the same Gaussian kernel. The smoothed neural activity was divided by the smoothed occupancy to calculate the spatial activity rate of each cell. Sessions in which the animal visited <50% of the binned arena space were excluded from spatial information analysis.

The spatial information content of a cell's activity (in bits) was defined as follows: $I = \Sigma_i(\lambda_i/\lambda) \times log_2(\lambda_i/\lambda) \times p_i$, where λ is the mean calcium activity ($\Sigma_i p_i \times \lambda_i$), λ_i is the mean calcium activity in the i-th pixel, and p_i is the probability of being in bin i (Skaggs et al., 1993; Rochefort et al., 2011; Shuman et al., 2020).

A place cell was defined as a cell whose spatial information fell above the 95th percentile of 500 shuffled trials. The shuffling procedure randomly selected a starting point from the animal's location vector, and then the spatial activity rates and spatial information content of each cell were recalculated. A cell's place field was defined as all contiguous bins with an activity rate at least half of the maximum, with the bin containing the maximum activity rate defined as the center of the place field.

Object responsiveness

Object responsiveness of hippocampal neurons was calculated using an object responsiveness index (ORI) and defined as ORI = $(A_O - A_A)/(A_O + A_A)$, with A_O being the mean calcium activity within two spatial bins (5 cm) around the object center and A_A being the mean calcium activity of all arena bins outside the object space (Deshmukh and Knierim, 2011, 2013). Cells with a positive ORI were labeled as "object responsive."

Statistics

Statistical analysis was conducted using OriginPro 2016 and MATLAB 2016b. Data are presented as mean ± SEM. Error bars and line shading, where present, represent SEM. Nonparametric statistical tests were used if assumptions of parametric statistics were violated. ANOVAs, t tests, and Mann–Whitney were performed using two tails.

Results

Optogenetic cerebellar stimulation impairs performance specifically on a spatial memory task

To investigate whether acute perturbations of the cerebellar cortex interfere with a hippocampal-dependent cognitive task, we used two behavioral assays. One assay, the OLM test, relies on spatial memory and is sensitive to hippocampal dysfunction; the other assay, the ORM test, relies on memory of object identity and is generally insensitive to hippocampal dysfunction (Mumby et al., 2002; Winters et al., 2004; Winters and Bussey, 2005; Balderas et al., 2008; Haettig et al., 2011). A benefit of using these two tasks is their parallel structure. Both tasks rely on the animals' natural interest in novelty and involve exposing the animals to two identical objects on day 1 (training). The following day (testing), a novelty is introduced: either a familiar object moved to a novel location (OLM) (Fig. 1*a*) or a novel object in place of a familiar object (ORM) (Fig. 1*f*). Animals that recognize the novelty (i.e., remember the previous object locations/object identities) will spend more time investigating the novel location/object compared with the unchanged location/object, resulting in a high DI. PV-ChR mice, which express ChR in PV-expressing cells throughout the brain, including cerebellar Purkinje cells and inhibitory hippocampal PV cells, were initially used in these tasks. In both tasks, a light stimulus (blue light, ~7 Hz, 3 s duration, 33% duty cycle; chosen to match parameters used in previous work) (Krook-Magnuson et al., 2014) was delivered every 60 s for both training and testing.

Optogenetic activation of the cerebellum produced a marked impairment on the OLM task (Fig. 1*b*). A deficit was evident with either vermis stimulation (vermis opsin-negative $N = 8$ animals, DI = 26.8 ± 5.5; opsin-positive $N = 11$, DI = 5.7 ± 3.5, p = 0.014, Mann–Whitney) or simplex stimulation (simplex opsin-negative $N = 10$ animals, DI = 20.6 ± 3.4; opsin-positive $N = 11$ animals, DI = 4.7 ± 3, $p = 0.01$, Mann–Whitney), indicating that cerebellar manipulation can interfere with performance on a hippocampal-dependent spatial memory task.

This deficit was because of cerebellar manipulation, rather than an off-target effect of light delivery, as control (opsin-negative) animals receiving the same light delivery showed a strong preference for the moved object (Fig. 1*b*).

Previous studies have suggested that the OLM task, while strongly hippocampal dependent (Broadbent et al., 2004), may be resilient to manipulation of PV cells. Specifically, Shuman et al. (2020) found no effect on information content, stability, or place cell percent when chemogenetically inhibiting hippocampal PV cells (despite an increase in overall activity of recorded cells). Similarly, Hijazi et al. (2019) chemogenetically inhibited hippocampal PV neurons during training on a Morris Water Maze and found no learning or memory deficits in healthy mice. Perhaps most relevant to our work, Wang et al. (2018b) chemogenetically excited hippocampal PV neurons, including in healthy animals, and found no impact on the DI in an object-location memory task. Therefore, optogenetic stimulation of hippocampal PV cells provided us with a useful additional point of comparison. Specifically, optogenetic activation of hippocampal PV cells did not produce a significant deficit on the OLM task (opsin-negative $N = 13$, mean DI = 20.1 ± 5.1; opsin-positive N = 11, mean = 17.6 ± 4, $p = 0.56$, Mann–Whitney) (Fig. 1*b*). This further indicates that light-delivery per se did not underlie the effects observed with cerebellar modulation. Moreover, these findings support that the effects seen with cerebellar manipulation are particularly robust, as even certain manipulations directly to the hippocampus fail to produce as severe an effect.

As the cerebellum is a canonically motor structure, and as manipulation of the cerebellum can produce motor effects, which could theoretically interfere with an animal's ability to perform the OLM task, we performed additional analyses and experiments. First, we examined the total time investigating objects (both objects combined), to ensure that animals were able to move around and investigate objects. There were no differences between opsin-positive animals and their opsin-negative controls in overall investigation time, regardless of stimulation site (vermis-targeted opsin-positive vs opsin-negative: $p = 0.5$, Mann–Whitney; simplex-targeted opsin-positive vs opsin-negative: $p = 0.38$, Mann–Whitney) (Fig. 1*c*). Instead, the relative time spent investigating the novel versus familiar object locations was impacted (simplex opsin-negative mean time investigating

familiar object = 3.2 ± 0.6 s, time investigating novel object = 5.0 ± 1.0, $p = 0.02$, paired t test; simplex opsin-positive mean time investigating familiar object = 2.9 ± 0.4, time investigating novel object = 3.2 ± 0.4, $p = 0.2$, paired t test; vermis opsin-negative time investigating familiar object = 1.9 ± 0.3, time investigating novel object = 3.6 ± 1, $p = 0.03$, paired t test; opsin-positive $N = 10$, time spent investigating familiar object = 1.9 ± 0.3, time investigating novel object = 2.7 ± 0.2, $p = 0.1$, paired t test) (Fig. 1*d*,*e*). The lack of difference in total investigation time, with an obvious difference in relative investigation time, indicated that the ability of the animals to investigate the objects was intact, and therefore that the deficit on the OLM task with cerebellar stimulation was unlikely to be due simply to motor effects.

Further evidence of competent task-related motor abilities came from performance on the ORM test. As noted above, the ORM task parallels the OLM task in structure. If the deficit on the OLM task were because of motor effects, or indeed other explanations, such as altered motivation or reduced interest in novelty, one would anticipate a similar deficit on the ORM task. However, cerebellar manipulation did not produce a deficit on the ORM task (vermis-targeted: opsin-negative $N = 11$ mice, DI = 20.1 ± 2.5; opsin-positive $N = 16$ mice, DI = 21.4 ± 5.2, $p = 0.6$, Mann–Whitney; simplex-targeted mice: opsin-negative $N = 12$ mice, DI = 23.8 ± 5.5; opsin-positive $N = 15$ mice, DI = 18.6 ± 2.9, $p = 0.54$, Mann–Whitney) (Fig. 1*g*), nor did activation of hippocampal PV cells impair ORM performance, as expected (opsin-negative $N = 17$ mice, DI = 19.3 ± 6.2; opsin-positive $N = 15$ mice, DI = 19.3 ± 5.4; $p = 0.95$, Mann–Whitney). Also, as seen for the OLM task, opsin-positive and opsin-negative mice exhibited similar total investigation times (vermis-targeted opsin-positive vs opsin-negative $p = 0.47$, Mann–Whitney; simplex-targeted opsin-positive vs opsin-negative $p = 0.98$, Mann–Whitney) (Fig. 1*h*). These results indicate that intermittent activation of the cerebellar cortex did not significantly impair the animals' ability or motivation to investigate novel objects. Acute optogenetic excitation of the cerebellum specifically disrupted discrimination of a spatially novel object location, a hippocampal function.

While these results clearly indicate that cerebellar manipulation can impact performance on a hippocampal-dependent task, and while Purkinje cells express PV and thus channelrhodopsin in our experiments, other neuron types (i.e., molecular layer interneurons) in the cerebellum also express PV. To determine whether optogenetic excitation of Purkinje cells selectively is able to reproduce deficits on the OLM task, we additionally tested optogenetic excitation of the vermis in animals with opsin expression in the cerebellum restricted to Purkinje cells (i.e., Pcp-ChR animals). Light delivery to animals with this highly restricted opsin expression recapitulated results seen in PV-ChR animals: optogenetic excitation of the cerebellum produced a strong deficit on the OLM task (OLM: opsin-negative $N = 8$ mice, DI = 23 ± 7; opsin-positive $N = 8$ mice, DI = 4.5 ± 5; $p = 0.04$, Mann–Whitney) without changing total investigation times (opsin-negative mean = 7.3 ± 1.3 s, opsin-positive mean = 5.9 ± 0.9 s, $p = 0.49$, Mann–Whitney) nor performance on the ORM task (ORM: opsin-negative $N = 9$, DI = 17 ± 3.5; opsin-positive $N = 8$, DI = 17.5 ± 5.4; $p = 0.59$, Mann–Whitney) or ORM investigation time (opsin-negative mean = 15.3 ± 0.9 s, opsin-positive mean = 10.9 ± 1.6 s, $p = 0.06$, Mann–Whitney) (Fig. 1*i*–*l*). Therefore, selective manipulation of Purkinje cells is sufficient to induce behavioral deficits on the OLM task.

Cerebellar modulation evokes hippocampal LFP changes

While optogenetic modulation of the cerebellum produced deficits on a hippocampal-dependent task, it remained possible that the observed deficits on the OLM task were because of effects downstream of the hippocampus (i.e., that the cerebellum is unable to actually influence the hippocampus itself). To better determine whether the cerebellum could impact the hippocampus, we recorded LFPs in the hippocampus while optogenetically manipulating the cerebellum in Pcp-ChR animals. In order to additionally monitor effects in the cerebellum itself, we simultaneously recorded LFP also from the cerebellum (Fig. 2*a*,*b*). We examined both the effect of the light parameters used in behavioral experiments (and in later experiments), as well as shorter light pulses (10 ms), which produced a smaller effect but allowed us to investigate a broader range of stimulation frequencies (Extended Data Figs. 2-1, 2-2, 2-3, 2-4, 2-5).

Light delivery to the cerebellum resulted in evoked hippocampal potentials (Fig. 2). This provides strong evidence that acute cerebellar modulation can impact the hippocampus per se. Across a broad range of frequencies, these evoked potentials followed the frequency of light delivery to the cerebellum (Fig. 2; Extended Data Figs. 2-1, 2-2, 2-3, 2-4, 2-5). To determine the latency to hippocampal response, we examined the hippocampal LFP responses to 1 Hz stimulation, which revealed a latency between stimulus onset and the first peak in hippocampal LFP response of 16.1 ± 0.95 ms for vermis stimulation and 13.6 ± 0.92 ms for simplex (vermis vs simplex latency, $p = 0.17$, t test). This suggests a multisynaptic pathway by which the cerebellum and hippocampus are functionally connected, consistent with recent studies (Yu and Krook-Magnuson, 2015; Bohne et al., 2019; Watson et al., 2019; Krook-Magnuson, 2020).

Simultaneously recording from the cerebellum (in addition to the hippocampus) allowed direct confirmation that light delivery modulated the cerebellum, and allowed comparisons of cerebellar responses across stimulation frequencies and across locations (simplex vs vermis). Light delivery to the vermis or simplex produced similar changes in cerebellar LFP power (Fig. 2*c*,*d*), with both groups showing increasing effects at higher frequencies ($N = 6$ control, 6 vermis-targeted, 5 simplex-targeted animals; mixed-effects ANOVA: main effect of group $F = 13.4$, df = 2, $p = 4.1E\text{-}6$; control vs vermis: $p = 1.3E\text{-}4$; control vs simplex: $p = 1.9E10\text{-}6$; vermis vs simplex: $p = 0.2$; main effect of frequency $F = 7.7$, df = 9, $p = 3.5E\text{-}9$) (Figs. 2*d*; Extended Data Figs. 2-1, 2-2, 2-3, 2-4, 2-5). This suggests that the cerebellum may be particularly influenced by higher-frequency light delivery, but, notably, did not reveal any significant vermis versus simplex differences (cerebellar LFP responses, vermis vs simplex: $p = 0.2$).

Mimicking effects in the cerebellum, changes in hippocampal power (measured at the stimulus frequency) generally increased with higher stimulation frequencies (Fig. 2*e*). However, vermis targeting produced a greater hippocampal response than targeting the simplex (mixed-effects ANOVA: main effect of group $F = 4.84$, df = 2, $p = 0.04$; main effect of frequency: $F = 2.3$, df = 9, $p = 0.02$, group × frequency interaction $F = 1.8$, df = 18, $p = 0.03$; control vs simplex $p = 0.03$, control vs vermis $p = 0.00005$, vermis vs simplex $p = 0.01$) (Fig. 2*e*).

When the cerebellum was stimulated with the same parameters used in behavioral experiments (50 ms light pulses), robust effects were observed both in the cerebellum and, importantly, the hippocampus. Light delivery produced large changes in hippocampal spectral power in both simplex- and vermis-targeted groups, but not opsin-negative controls (control, $N = 6$ animals, mean increase in power at stimulation frequency = 5 ± 4%; simplex, $N = 4$ animals, mean = 85 ± 31%; vermis $N = 5$ animals mean = 421 ± 301%, $p = 0.003$, Kruskal–Wallis ANOVA; vermis vs control: $p = 0.008$, simplex vs control: $p = 0.01$, vermis vs

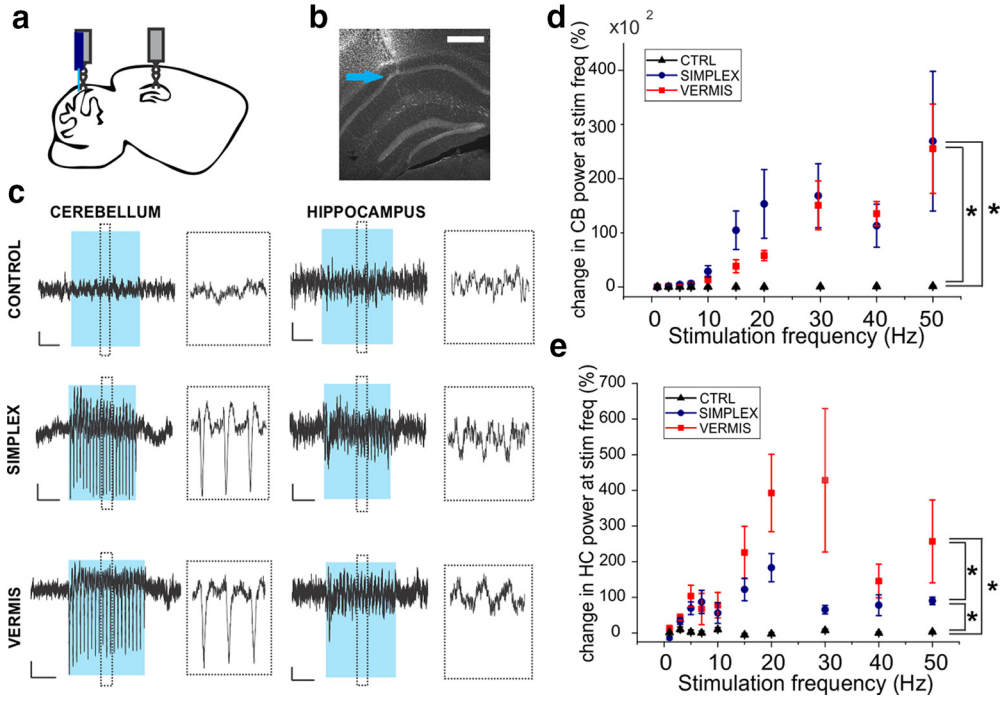

Figure 2. Cerebellar stimulation evokes hippocampal LFP responses. ***a***, Schematic illustration of locations of hippocampal electrode (dorsal hippocampus) and cerebellar optrode (vermis or simplex). ***b***, Example image showing hippocampal electrode tract (blue arrow). Scale bar, 0.5 mm. ***c***, Example traces of averaged LFP recordings from 7 Hz stimulation (10 ms pulse width). Left, Cerebellar electrode. Right, Hippocampal electrode. Blue bar represents light delivery period. Dashed lines indicate the ~500 ms of data expanded in inset. Calibration: 1s, 5 μV. ***d***, Percent change in power at the stimulation frequency in the cerebellar LFP. *$p < 0.001$ (mixed-effect ANOVA). ***e***, Percent change in power at the stimulation frequency in the hippocampal recording. *$p < 0.01$ (mixed-effect ANOVA). Black represents opsin-negative control animals. Blue represents opsin-expressing animals with light delivered to the simplex. Red represents opsin-expressing animals with light delivered to the vermis. Cerebellar stimulation, especially the vermis, caused an increase in hippocampal LFP power. Spectrograms of averaged hippocampal and cerebellar responses are available in Extended Data Figs. 2-1, 2-2, 2-3, 2-4, and 2-5.

simplex $p = 0.06$, Mann–Whitney) (Extended Data Figs. 2-1, 2-2, 2-3, 2-4, 2-5).

These data provide strong evidence that cerebellar manipulation can have strong effects not only on a hippocampal-dependent task, but also on the hippocampus itself.

Cerebellar excitation alters hippocampal cFos expression

To capture a snapshot of how different regions of the hippocampus respond to these two different sites of cerebellar modulation, we examined hippocampal cFos expression after cerebellar stimulation (Fig. 3). cFos is an immediate early gene and transcription factor observed following increases in neuronal activity, and can be interpreted as an indicator of recently active cell populations (Flavell and Greenberg, 2008; Minatohara et al., 2016). Experimental animals were paired with a control animal, then both subjected to light stimulation, perfused, and tissue then immunoprocessed for *cFos* (Fig. 3*a–d*). Repeated optogenetic stimulation of the cerebellar cortex (using the same light parameters as used in the behavioral experiments) for 1 h produced restricted and specific changes in hippocampal $cFos^+$ cell counts in both vermis- and simplex-targeted animals (Fig. 3).

Vermis-targeted ($N = 7$ pairs) animals had significantly elevated cFos counts in CA1 alveus/stratum oriens layers (mean = 399 ± 107% cFos-positive cells relative to controls, $p = 0.015$, Signed-Rank Test), CA1 stratum pyramidale (i.e., the pyramidal cell layer) (mean = 381 ± 119%, $p = 0.015$, Signed-Rank Test), and, to a smaller extent, CA3 stratum pyramidale (mean = 176 ± 26%, $p = 0.015$, Signed-Rank Test) (Fig. 3*f*). Simplex-targeted ($N = 7$ pairs) animals had significantly elevated $cFos^+$ counts in the dentate gyrus molecular (i.e., inhibitory neuron) layer (mean = 181 ± 16%, $p = 0.031$, Signed-Rank Test) and reduced $cFos^+$ cell counts in CA3 stratum lucidum/radiatum/moleculare (mean = 53 ± 14%, $p = 0.046$, Signed-Rank Test) (Fig. 3*e*). Notably, neither group showed elevated cFos expression in the dentate gyrus granule cell layer.

These results indicate that specific hippocampal subregions respond to cerebellar stimulation and that modulation of different aspects of the cerebellar cortex can produce differential responses.

Altered activity of hippocampal cells during and following cerebellar stimulation

To observe how individual CA1 cells respond to cerebellar stimulation while simultaneously monitoring a large number of cells, we recorded calcium activity from GCaMP6f-infected hippocampal CA1 neurons in Pcp-ChR mice using a one-photon microendoscope (Miniscope) in freely moving animals ($N = 9$ animals; 4 control, 5 opsin-positive) (Fig. 4*a–c*). The animals were subjected to an object-exploration task while light was intermittently delivered to the cerebellum, using the same light-delivery protocol as used in the previous behavioral tasks. The design of the task was modeled after the OLM task, including a training day with two identical objects and a testing day with a moved object, but this object-exploration task incorporated a larger arena to better reveal spatial-related activity and more exposure time to allow for more observations.

First, raw (i.e., not deconvolved) calcium traces were aligned to stimulus onset to identify changes related to cerebellar stimulation (Fig. 4*d–g*). Light delivery produced a transient but overall nonsignificant decrease in the calcium signal during the stimulus

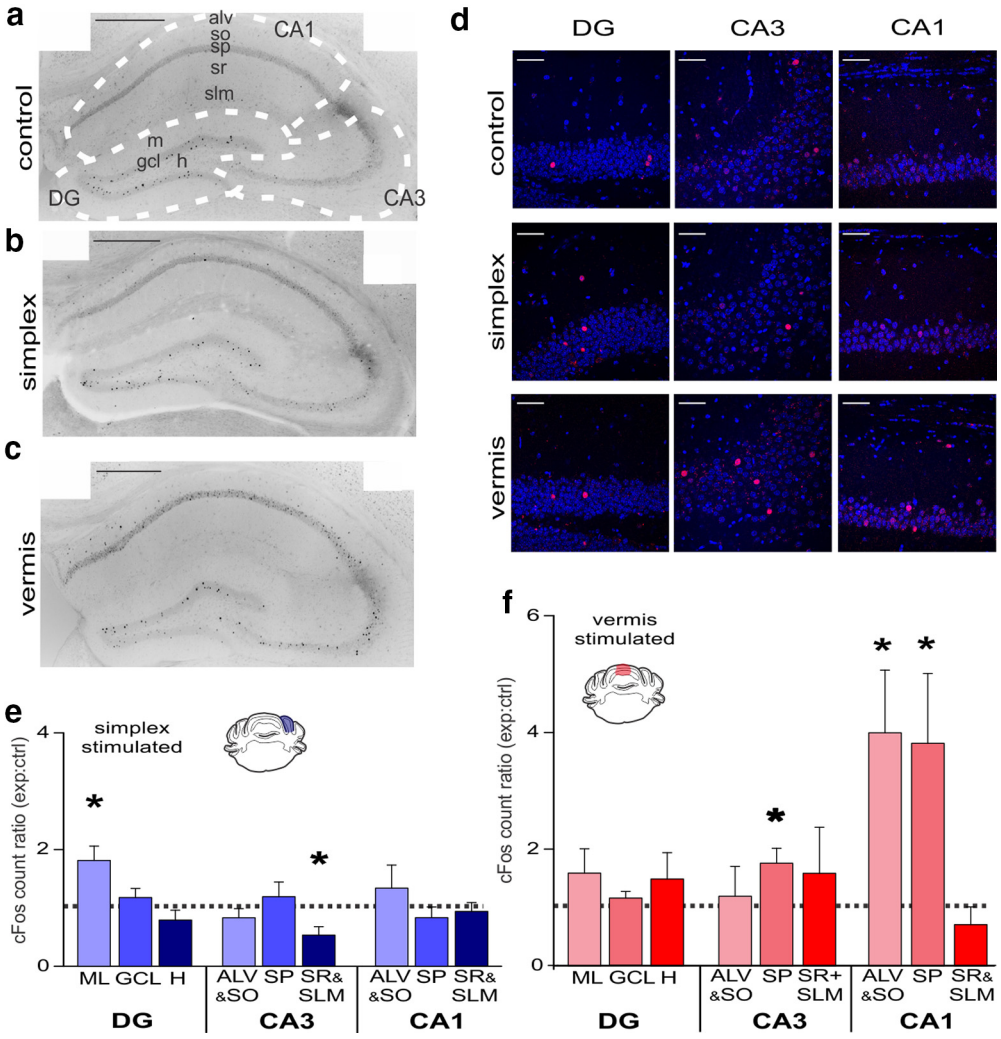

Figure 3. Selective changes to hippocampal cFos expression following cerebellar stimulation. ***a***, Coronal image of hippocampus from a control animal following cerebellar light delivery, processed for cFos immunohistochemistry. Dotted lines and labels indicate hippocampal subregions used for analysis. Scale bar, 0.5 mm. ***b***, Same as in ***a***, from a simplex-targeted opsin-expressing animal. ***c***, Same as in ***a***, from a vermis-targeted opsin-expressing animal. ***d***, Fluorescent images showing cFos expression (red) in different aspects of the hippocampus, following light. Blue represents DAPI. Scale bar, 50 µm. ***e***, cFos expression in simplex-targeted mice normalized to paired opsin-negative controls. *$p < 0.05$ (Signed-Rank test). ***f***, Same as in ***e***, but for vermis-targeted mice. *$p < 0.05$ (Signed-Rank test). Vermis-targeted animals displayed an especially strong increase in cFos in both CA1 pyramidale and alveus/oriens. ml, Molecular layer; gcl, granule cell layer; h, hilus; alv, alveus; so, stratum oriens; sp, stratum pyramidale; sr, stratum radiatum; slm, stratum lacunosum moleculare; DG, dentate gyrus; CA, cornu ammonis.

in opsin-positive animals versus controls (control, $n = 2153$ cells, mean area under the curve [AUC] during stimulus = 1 ± 2; simplex, $n = 1449$ cells, mean = 0.4 ± 4; vermis, $n = 1461$ cells, mean = -2.9 ± 3, Kruskal–Wallis ANOVA $p = 0.6$) (Fig. 4*f*). Following the offset of the light stimulus, there was a robust increase in fluorescence with both vermis- and simplex-targeting compared with controls (control mean AUC = -100 ± 9; simplex mean = 540 ± 13; vermis mean = 750 ± 13; $p = 4.4E\text{-}7$, Kruskal–Wallis ANOVA; vermis vs control $p = 8.4E\text{-}7$, simplex vs control $p = 6.3E\text{-}5$, vermis vs simplex $p = 0.4$, Mann–Whitney) (Fig. 4*g*).

The changes in the calcium signals could be because of changes in calcium event rate and/or event amplitude. In order to better investigate what aspects of calcium activity were altered, the calcium transients were deconvolved to approximate their underlying bouts of neural activity (i.e., calcium "events"), providing higher temporal resolution than raw calcium transients because of the kinetics of the fluorescent calcium indicator (Pnevmatikakis et al., 2016). This enabled us to then examine frequency and amplitude of calcium events separately.

During the stimulus, both simplex- and vermis-targeted groups showed a significant decrease in event probability (i.e., rate) compared with controls (control mean change in event probability AUC = 2 ± 40; simplex mean = -328 ± 60; vermis mean = -225 ± 60; $p = 4.3E\text{-}5$, Kruskal–Wallis ANOVA; vermis vs control $p = 8.6E\text{-}4$, simplex vs control $p = 4.2E\text{-}5$, vermis vs simplex $p = 0.5$, Mann–Whitney) (Fig. 4*h*,*j*). Because the effect did not appear consistent for the entire duration of the stimulus, we asked whether there was a temporal component to the change in event probability during stimulus delivery. We compared the event probability during the first half of the stimulus to the second half. The control group showed no difference (first half mean AUC = 5 ± 20, second half = -2 ± 20, $p = 0.3$, Signed Rank Test). However, both the simplex- and vermis-targeted groups had significantly stronger changes during the first half of the stimulus compared with the second half (simplex: first half of the stimulus mean AUC = -217 ± 34, second half = -111 ± 30; vermis: first half of the stimulus mean AUC = -219 ± 30, second half = -5 ± 50; simplex first half vs second $p = 0.01$, vermis first half vs second $p = 9.3E\text{-}9$, Signed Rank Test), suggesting a transient or adapting response to light (Fig. 4*k*).

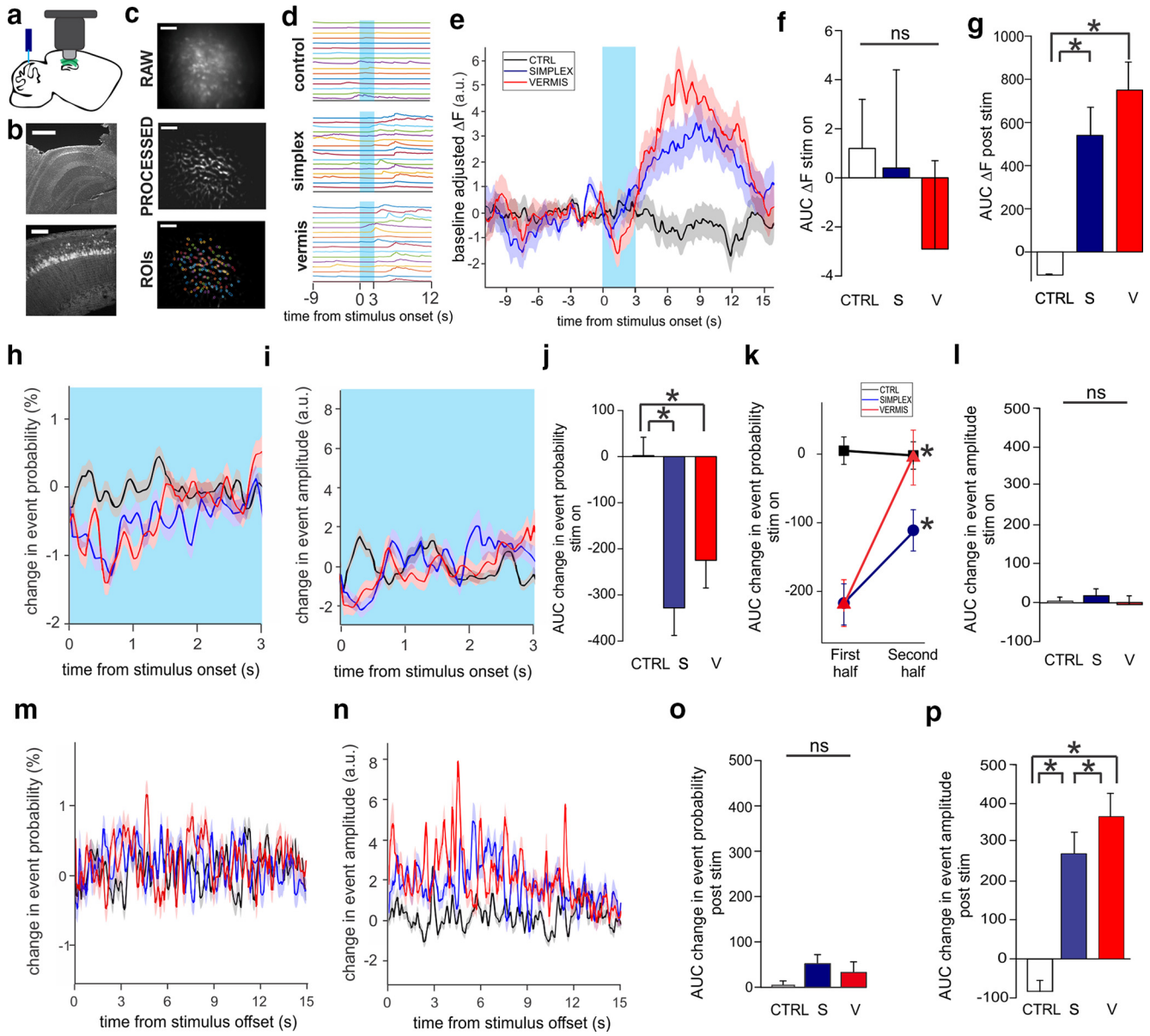

Figure 4. Cerebellar stimulation elicits changes in hippocampal calcium signals. ***a***, Schematic of experimental setup: optic fibers targeted to the cerebellum (simplex and vermis; blue), GCaMP6f-transduced dorsal hippocampus (green), GRIN lens implanted above CA1 (light gray), and microendoscope (Miniscope; dark gray) to record changes in calcium fluorescence. ***b***, Example images showing (top) GRIN lens implantation over hippocampus and (bottom) closeup of CA1 GCaMP6f expression. Scale bars: top, 0.5 mm; bottom, 0.1 mm. ***c***, Example miniscope FOV as a (top) raw image, (middle) background subtracted image, and (bottom) with automatically identified ROIs superimposed. Scale bars, 0.1 mm. ***d***, Example traces of raw calcium activity before, during, and after the stimulus. Each line indicates one example cell. Blue box represents stimulus period. ***e***, Changes in calcium fluorescence relative to average prestimulus baseline rate. ***f***, ***g***, Quantification of changes in fluorescence during stimulus period (***f***) and following stimulus offset (***g***). Note the strong postlight increases for simplex and vermis groups. *$p < 0.001$ (Mann–Whitney). ***h-l***, Changes to calcium event probability (***h***) and calcium event amplitude (***i***) during the stimulus (blue box). There is a decrease in event probability with simplex and vermis groups (***j***, $p < 0.001$, Mann–Whitney), which is especially transient with vermal stimulation (***k***; first half [1.5 s] of the stimulus compared with the second half, $p < 0.01$, Mann–Whitney). In contrast, there is no significant change in the event amplitude during the stimulus (***l***). ***m-p***, Changes to calcium event probability (***m***) or event amplitude (***n***) following stimulus offset. Although there is no significant change in the event probability post-light (***o***), there is a large increase in event amplitude following stimulation, which is especially strong for vermal stimulation. ***p***, *$p < 0.05$ (Mann–Whitney). ***e***, ***h***, ***i***, ***m***, ***n***, Shading represents SEM. CTRL, Control; S, simplex; V, vermis; a.u., arbitrary units. ns, not significant.

Event amplitude during the stimulus (Fig. 4*i*) was not significantly altered for any group (control mean AUC = 3 ± 10, simplex mean = 18 ± 20, vermis mean = −4 ± 20, $p = 0.2$, Kruskal–Wallis ANOVA) (Fig. 4*l*), indicating that the main effect during cerebellar stimulation was a decrease in rate.

In contrast, following stimulus offset, there was only a slight and nonsignificant increase in event probability (control mean AUC = 0.04 ± 0.12; simplex = 0.54 ± 0.2; vermis = 0.35 ± 0.22, $p = 0.06$, Kruskal–Wallis ANOVA) (Fig. 4*m*,*o*) but a marked increase in event amplitude with cerebellar stimulation (control mean AUC = −83 ± 30; simplex = 270 ± 60; vermis = 370 ± 60; $p = 1.2E\text{-}11$, Kruskal–Wallis ANOVA; control vs simplex, $p = 6.8E\text{-}5$, control vs vermis, $p = 7.1E\text{-}11$, Mann–Whitney) (Fig. 4*n*, *p*). This indicates a rebound effect following light, which is distinct from acute effects during light delivery.

Interestingly, vermis-stimulated animals displayed a greater poststimulus increase in calcium event amplitude than simplex-stimulated animals (vermis vs simplex, $p = 0.03$, Mann–Whitney)

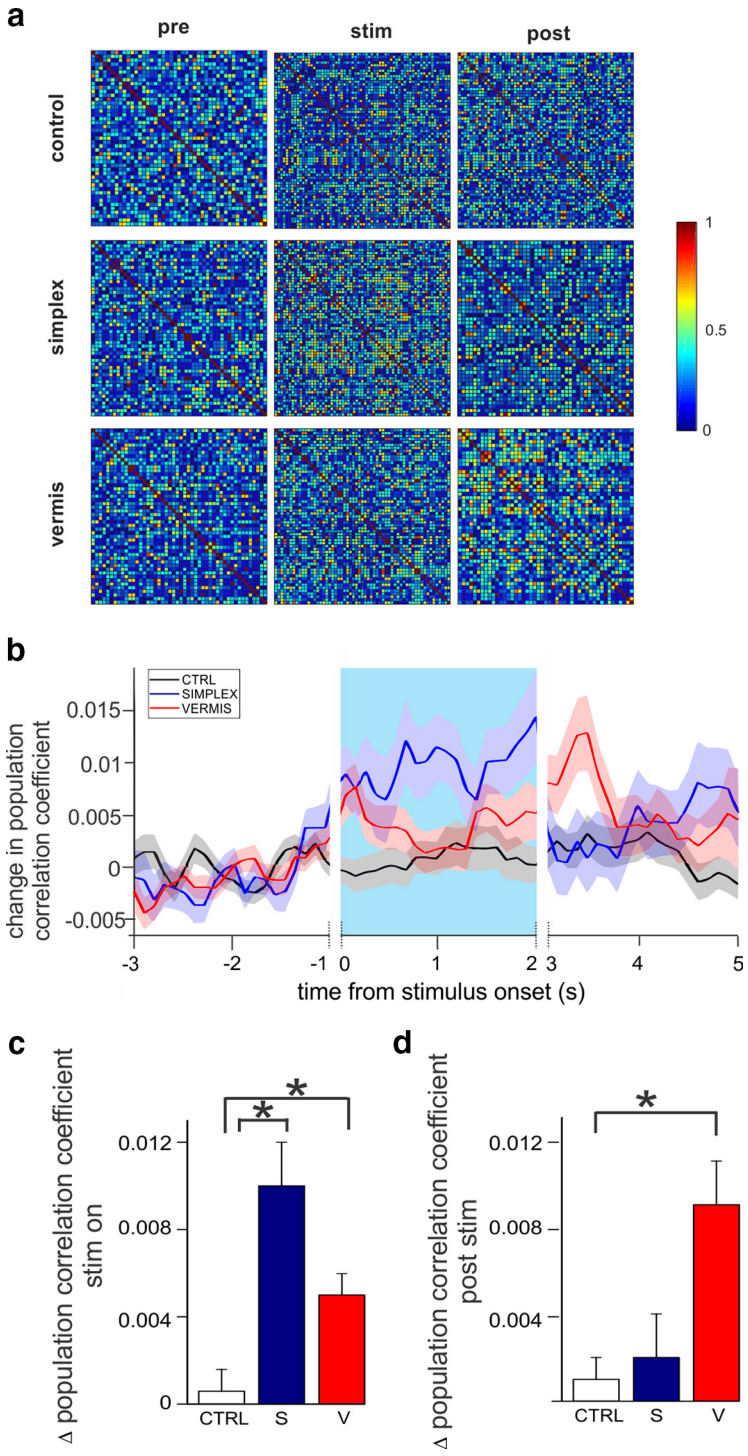

Figure 5. Increased correlation coefficient across hippocampal CA1 with cerebellar stimulation. ***a***, Example absolute value correlation coefficient matrices of active cells during a 1 s period before, during, and after a light stimulus (pre, stim, and post, respectively) in a control (top), simplex-stimulated (middle), or vermis-stimulated animal (bottom). Each cell is represented on the *x* and *y* axis. Diagonal indicates autocorrelation. Hotter colors represent higher correlation levels, as shown by the scale bar on the right. ***b***, Plot of changes to global correlation coefficient relative to prestimulus correlation levels. Blue box represents stimulus period. Breaks in *x* axis come from 1 s moving window to calculate the correlation coefficient. Shading represents SEM. ***c***, ***d***, Mean changes to correlation measures during the stimulus period (***c***) or poststimulus period (***d***). Both simplex and vermis stimulation resulted in increased correlation during the stimulus period (***c***). Correlation measures also strongly increased following light delivery to the vermis (***d***). *$p < 0.01$ (Mann–Whitney). CTRL, Control; S, simplex; V, vermis.

(Fig. 4*p*), again suggesting a greater impact of vermal (rather than simplex) stimulation on the hippocampus.

In summary, we observed an abrupt and transient decrease in event probability at stimulus onset with both simplex and vermis modulation, followed by a longer-lasting increase in fluorescence, particularly with vermal modulation, after stimulus offset, which was driven by enhanced event amplitude. These data show both rapid and more lasting effects of cerebellar stimulation on hippocampal activity.

Increased correlated activity of hippocampal cells with cerebellar stimulation

As cerebellar stimulation appeared to produce changes across a large number of hippocampal cells, we wondered whether the correlated activity between hippocampal cells was affected by cerebellar stimulation. We therefore calculated the correlation coefficients between pairings of all active cells prior, during, and after each stimulus (control $n = 136$ light stimuli, simplex $n = 60$, vermis $n = 64$) (Fig. 5*a*).

During the stimulus window, the mean correlation of activity significantly increased from baseline in both simplex-targeted and vermis-targeted groups but not in controls (change in control mean absolute values of correlation coefficients, light vs baseline = 0.00059 ± 0.001; simplex = 0.01 ± 0.002; vermis = 0.005 ± 0.001; $p = 0.002$, Kruskal–Wallis ANOVA; simplex vs control $p = 0.0005$, vermis vs control $p = 0.01$; simplex vs vermis $p = 0.17$, Mann–Whitney) (Fig. 5*b*,*c*). This suggests that optogenetic stimulation of the simplex or vermis may cause widespread coordinated changes of activity in the hippocampus during light delivery.

Following stimulus offset, however, a different pattern emerged. Correlated activity in vermis-targeted animals was significantly elevated immediately (1 s) following the stimulus, whereas the simplex-targeted group had returned to baseline levels (change in control mean correlation coefficient, stimulus offset vs baseline = 0.001 ± 0.001; simplex = 0.002 ± 0.002; vermis = 0.009 ± 0.002; $p = 0.03$, ANOVA; vermis vs control $p = 0.01$, vermis vs simplex $p = 0.056$, simplex vs control $p = 0.8$, t test) (Fig. 5*b*, *d*). This suggests a possible rebound effect after stimulation in vermis-targeted animals and highlights an additional difference between vermis and simplex modulation.

Together, these results show rapid effects of cerebellar manipulation on the coordinated activity of hippocampal CA1 neurons and additional alterations following stimulus offset specifically with vermis targeting.

Altered hippocampal object-location processing and place cell expression with cerebellar modulation in an object-exploration task

Given the observed spatial processing deficits suggested by the OLM task (Fig. 1), and the altered activity levels suggested by cFos measures (Fig. 3) and calcium imaging (Fig. 4), we next asked what effect acute manipulation of the cerebellum could have on hippocampal object interactions and place fields. Notably, there were no significant differences between groups in distance traveled during training or testing sessions (training session: control = 1653 ± 194 cm, $n = 7$ sessions; simplex = 1672 ± 237 cm, $n = 4$; vermis = 1628 ± 205 cm, $n = 5$; $p = 0.9$, ANOVA; testing session: control = 1886 ± 220 cm, $n = 8$; simplex = 1803 ± 350 cm, $n = 5$; vermis = 1682 ± 173 cm, $n = 5$; $p = 0.8$, ANOVA), with all groups showing good coverage of the arena space (Fig. 6*a*). Therefore, both groups showed similar mobility and ability to explore the arena and its contents.

Given that the presence of objects in an environment is known to affect the activity of hippocampal CA1 neurons (Komorowski et al., 2009; Burke et al., 2011), we examined the responsiveness of cells in areas near an object while the animals freely moved about the environment. During the training session, the control group had significantly more cells with increased activity near an object than either the simplex-stimulated or vermis-stimulated groups (control object responsive cells = 59% [613 of 1045]; simplex-stimulated object responsive cells = 45% [257 of 563]; vermis-stimulated object responsive cells = 42% [247 of 580]; vermis vs control $p = 3.2E\text{-}6$, simplex vs control $p = 6.5E\text{-}4$, simplex vs vermis $p = 0.31$, Fisher Exact Test) (Fig. 6*b*). These data suggest that cerebellar stimulation could lead to aberrant object-location processing.

When examining responsiveness to object locations during the testing session, a similar proportion of cells were responsive to the unmoved object's location across groups (control object responsive cells = 38% [383 of 1004]; simplex-stimulated object responsive cells = 38% [168 of 437]; vermis-stimulated object responsive cells = 39% [226 of 580]; vermis vs control $p = 0.7$, simplex vs control $p = 0.8$, simplex vs vermis $p = 0.9$, Fisher Exact Test) (Fig. 6*c*). In contrast, there were prominent differences in the percentage of cells responsive to the moved object's location between groups (Fig. 6*d*); the control group had a significantly higher proportion of cells preferentially active near the moved-object's new location than either cerebellar-stimulated group (control object responsive cells = 37% [371 of 1004], simplex-stimulated object responsive cells = 31% [141 of 437], vermis-stimulated object responsive cells = 25% [145 of 563]; control vs vermis $p = 9.2E\text{-}7$, control vs simplex $p = 0.024$, Fisher Exact Test). Additionally, the simplex-stimulated group had a larger percent of cells preferentially active near the moved object's location than the vermis-stimulated group, suggesting a stronger impact of vermis stimulation on hippocampal function (vermis vs simplex $p = 0.04$, Fisher Exact Test) (Fig. 6*d*).

Of the total population of cells recorded, individual cells with significant spatial tuning (i.e., place cells; for details, see Materials and Methods) were identified and subjected to further analysis. During both the training and testing sessions, place cells had similar place field sizes across groups (training session: control $n = 42$ place cells, mean = 59 ± 5 cm^2; simplex $n = 30$, mean = 67 ± 6; vermis $n = 19$, 59 ± 8; $p = 0.5$, ANOVA; testing session: control $n = 50$ place cells, mean = 59 ± 7 cm^2; simplex $n = 28$,

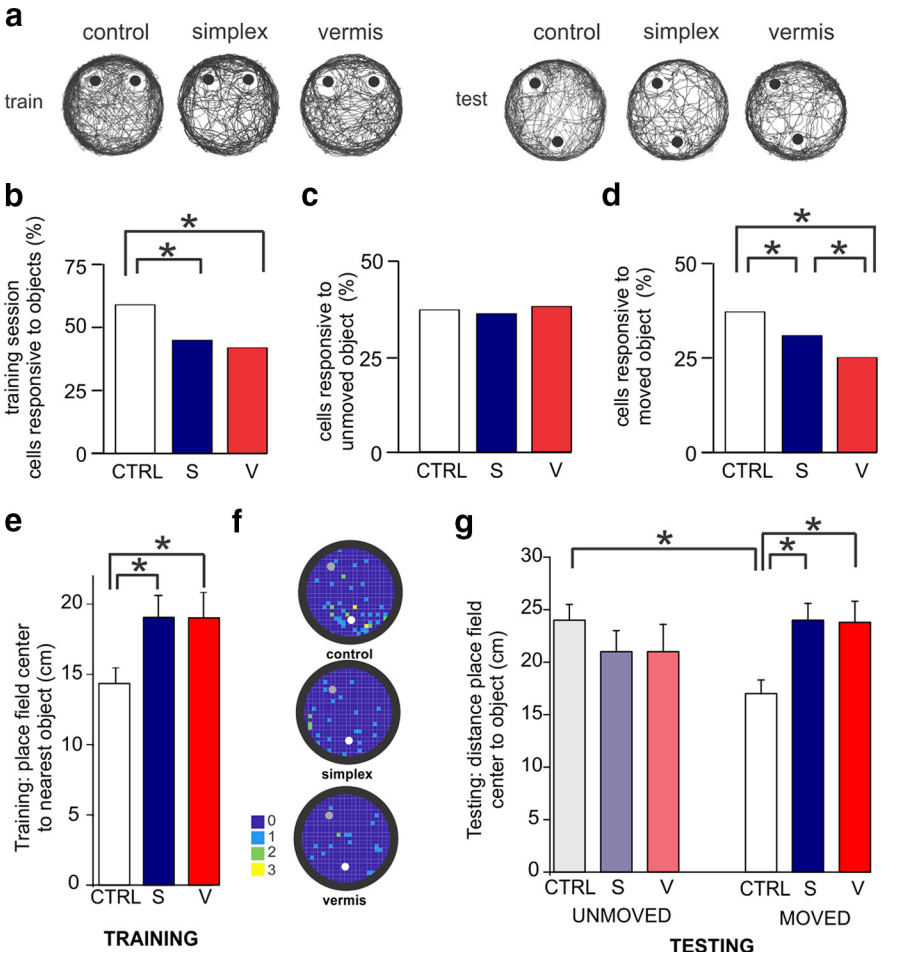

Figure 6. Cerebellar stimulation alters object-place dynamics in hippocampal cells. ***a***, Location across animals in the arena. Circles represent object location. All groups covered large swaths of the arena. ***b***, Proportion of cells that are responsive to the objects in the training session. Note the decreased responsiveness in simplex and vermis groups relative to controls. *$p < 0.05$ (Fisher Exact test). ***c***, Same as in ***b***, but for responsiveness to the unmoved object during the testing session. ***d***, Same as in ***c***, but for responsiveness to the moved object. Note the decreased responsiveness of simplex and vermis groups relative to controls. *$p < 0.05$ (Fisher Exact test). ***e***, Quantification of the distance between place fields and the nearest object during the training session. Control group place fields were closer to objects. *$p < 0.05$ (Mann–Whitney). ***f***, Representation of location of place field centers recorded across all animals during the testing session relative to the location of the moved and unmoved objects. Gray (top) and white (bottom) circles represent locations of the unmoved and moved objects, respectively. Color bar represents number of place fields observed in that spatial bin. Note the clustering of place fields near the moved object in controls. ***g***, Quantification of the distance between the place field center and each object during the testing session. Place cells from control animals were closer to the moved object than the unmoved object; place cells from simplex- and vermis-targeted animals were not. *$p < 0.05$ (*t* test). CTRL, Control; S, simplex; V, vermis.

mean = 62 ± 6; vermis $n = 18$, mean = 52 ± 7; $p = 0.7$, ANOVA). While trending, there were also no significant differences in the information scores of place cells across groups (training: control mean information score = 1.45 ± 0.14 bits, simplex mean = 1.25 ± 0.08 bits, vermis mean = 1.78 ± 0.21 bits, $p = 0.08$, Kruskal–Wallis ANOVA; testing session: control mean information score = 1.87 ± 0.09 bits, simplex mean = 1.66 ± 0.14 bits, vermis mean = 1.78 ± 0.21 bits, $p = 0.07$, Kruskal–Wallis ANOVA).

However, there were significant and interesting differences in the locations of the place fields relative to the objects (Fig. 6*e–g*). During the training session, place cells of control animals were significantly closer to objects than place cells from cerebellum-stimulated animals (control, $n = 42$ place fields, mean place field distance to nearest object = 14.3 ± 1.2 cm; simplex, $n = 30$ place fields, 19 ± 1.6 cm; vermis, $n = 19$ place fields, 19 ± 1.9 cm; $p = 0.03$, Kruskal–Wallis ANOVA; control vs vermis $p = 0.047$, control vs simplex $p = 0.023$, simplex vs vermis $p = 0.9$, Mann–Whitney) (Fig. 6*e*).

During the testing session, controls showed place fields closer to the moved object location than to the unmoved object ($p = 4.7\text{E-}4$, t test) (Fig. 6*f*,*g*). Place fields from simplex- or vermis-targeted animals, in contrast, did not show this bias toward the novel object location (simplex: $p = 0.24$; vermis: $p = 0.5$, t test) (Fig. 6*f*,*g*). Overall, while the distance between place fields and the unmoved object was similar between groups (control mean = 24 ± 1.5 cm, simplex mean = 21 ± 2 cm, vermis mean = 21 ± 2.6 cm; $p = 0.38$, ANOVA), controls showed place fields closer to the moved object than cerebellar stimulated animals (control mean = 17 ± 1.3 cm, simplex mean = 24 ± 1.6, vermis mean = 23.8 ± 2, $p = 0.001$, ANOVA; simplex vs control $p = 9.2\text{E-}4$, vermis vs control $p = 0.01$, simplex vs vermis $p = 0.7$, t test) (Fig. 6*f*,*g*). These findings suggest that cerebellar stimulation impacts hippocampal CA1 processing of object locations.

To additionally confirm these results, which used deconvolved signals, place cell identification and place field location analyses were repeated using instead raw calcium transients or event rate data. Both of these analyses revealed similar effects on place field location such that control, but not vermal or simplex-stimulated, animal's place cells were closer to the moved, compared with unmoved, object ($p < 0.03$, $p > 0.7$, $p > 0.2$, respectively, Mann–Whitney). Similarly, across all analyses, the average distance from place fields to the moved object was lower for controls compared with simplex ($p < 0.01$, Mann–Whitney) or vermis ($p < 0.05$, Mann–Whitney) stimulated animals. Therefore, findings were not sensitive to the specific methods of analysis implemented.

Together, the data collected in this study indicate a robust impact of cerebellar modulation, particularly strong for vermal modulation, on the hippocampus, which manifests at cellular, population, and functional levels.

Discussion

We set out to investigate whether and to what extent acute optogenetic excitation of the cerebellar cortex impacts hippocampal function in healthy mice. We found that modulation of the cerebellum induces a variety of changes in the hippocampus, including altered expression of *cFos*, evoked LFPs, modified hippocampal cell dynamics, and disrupted object-location processing in CA1. We investigated two different stimulation sites within the cerebellum: the midline vermis (lobule 4/5) and the simplex lobule. While effects from vermal and simplex targeting were largely similar, differences existed, with vermal stimulation generally producing stronger hippocampal modulation. This suggests that multiple areas of the cerebellum can influence hippocampal function, with distinct yet overlapping effects.

Acute cerebellar stimulation led to impairment on the OLM task, a spatial memory task that requires object-location discrimination and is hippocampal-dependent (Broadbent et al., 2004). Importantly, a similar impairment was not seen on the ORM task, a nonspatial memory task requiring object identity information. This difference in task performance suggests a fairly selective deficit. It also indicates that deficits on the OLM task cannot be explained by motor effects (which would have equally impacted the ORM task) nor motivational changes or a general disinterest in novelty or objects. Additionally, and in line with recent studies that chemogenetically manipulated hippocampal PV-expressing interneurons with subjects in a linear track (Shuman et al., 2020), water maze (Hijazi et al., 2019), or OLM task (Wang et al., 2018b), we did not find a spatial memory deficit with direct modulation of hippocampal PV-expressing interneurons. This underscores that effects seen on the OLM task with cerebellar manipulation are particularly robust and striking, and suggests a strong impact on hippocampal functioning.

While optogenetic manipulation is obviously not physiological (and comes with notable caveats, including synchronous impacts on neuronal populations), the cerebellum is being increasingly appreciated for its relationship to cognitive brain areas and tasks (Strick et al., 2009; King et al., 2019; Schmahmann, 2019) both in healthy and pathologic states, such as reward and addiction (Moulton et al., 2014; Wagner et al., 2017; Carta et al., 2019), social behavior and autism (Tsai et al., 2012; Peter et al., 2016; Badura et al., 2018; Gornati et al., 2018; Carta et al., 2019), and, particularly relevant to this study, spatial memory and navigation (Rochefort et al., 2013; King et al., 2019; Shipman and Green, 2019). Previously, studies examining the impact of chronic deficits in cerebellar plasticity, specifically loss of Purkinje cell LTP (Rochefort et al., 2011) or LTD (Lefort et al., 2019), found aberrant place cell representations in specific conditions. Similarly, a recent study using chemogenetic modulation of dopamine receptor 1-expressing cerebellar nuclear neurons found impaired spatial memory on the Barnes maze (Locke et al., 2018), further supporting the idea that the cerebellum can impact hippocampal function.

While object-location associations are at least partially mediated by other regions (Wang et al., 2018a), object-location association in the hippocampus appears to be especially critical, as the OLM task is strongly hippocampal-dependent (Winters and Bussey, 2005; Balderas et al., 2008). In our object-exploration task (Fig. 6), controls showed a greater CA1 representation of object locations during the training session than cerebellar stimulated animals. Additionally, during the testing session, controls, but not cerebellar manipulated animals, showed a higher density of place fields around the location of the moved object. These results provide key insight into the deficits observed on the OLM task with cerebellar manipulation; impairments on the OLM task with cerebellar manipulation likely reflect altered processing of object locations in CA1.

The hippocampus receives convergent information about objects (classically thought to be routed through the perirhinal and lateral entorhinal cortices) (Kravitz et al., 2011; Knierim et al., 2014) and spatial and self-motion information (classically

thought to be routed through the parahippocampal and medial entorhinal cortex areas) (Barry and Burgess, 2014; Savelli and Knierim, 2019). As a result of this convergent information, hippocampal CA1 neurons and their place fields are sensitive to object-location associations, including objects in novel locations (Manns and Eichenbaum, 2009; Burke et al., 2011). Recent work has noted important distinctions along the septal-temporal (dorsal-ventral) axis (for review, see Strange et al., 2014), the distal-proximal axis (for review, see Igarashi et al., 2014), and along the radial (deep vs superficial) axis of the CA1 pyramidal cell layer (for recent review, see Soltesz and Losonczy, 2018; Valero and de la Prida, 2018). For example, lateral entorhinal cortex input is strongest to superficial (closer to stratum radiatum) and distal (closer to subiculum) CA1 pyramidal neurons, while medial entorhinal cortex input is particularly strong at deep, proximal, CA1 pyramidal neurons (Masurkar et al., 2017). Additionally, deep CA1 pyramidal cells receive stronger input from CA2 (Valero et al., 2015), are more likely to show burst firing (Mizuseki et al., 2011) (as are distal CA1 neurons) (Jarsky et al., 2008), and are strongly influenced by environmental features, such as landmarks (Danielson et al., 2016; Geiller et al., 2017). Notably, given our use of one-photon miniscopes, deep pyramidal cells are likely preferentially represented in our calcium imaging dataset.

In addition to altered densities of place fields around object locations, we observed rapid changes to hippocampal activity specifically at the time of cerebellar stimulation. Hippocampal local field changes were noted with light-onset to time-of-peak delays well under 20 ms. Calcium imaging experiments revealed a transient/depressing decrease in event rate with light delivery. During this period of decreased calcium signaling, we also observed an increase in coordinated activity across recorded CA1 neurons, seen as an increase in the calculated average correlation coefficients, suggestive of the activation of a population of inhibitory interneurons (which could both decrease activity rates and coordinate activity, and which fits with our cFos data).

Effects of light delivery were additionally observed at the offset of cerebellar stimulation. These effects included a substantial increase in GCaMP fluorescence, reflecting a robust increase in intracellular calcium. Interestingly, the increase in calcium fluorescence was strongly driven by an increase in event amplitude, with only a modest trend toward increased event rate. The amplitude of a fluorescent calcium event is linked to the number of temporally condensed action potentials (e.g., bursting) (Chen et al., 2013). Therefore, the increased fluorescence we observed immediately after cerebellar stimulation may reflect increased bursting of hippocampal neurons. Intracellular calcium and bursting are important signaling mechanisms that can strongly impact plasticity (Buzsáki, 1986; Chrobak and Buzsáki, 1996; Sneider et al., 2006), and may therefore be especially relevant to the observed hippocampal functional deficits. Notably, a recent study, which performed unit recordings and examined the impact of inhibition of Purkinje cells, also reported bursting in hippocampal neurons (Choe et al., 2018). Bursting, and increases in calcium signaling, may also be especially relevant to our cFos experiments (Morgan and Curran, 1986). Specifically, the strong increases in calcium event amplitude seen with stimulus offset may be driving the increased expression of cFos in CA1 neurons observed after vermal manipulation. In this regard, it is of particular interest that an increase in CA1 cFos expression was statistically significant only with vermal manipulation, and vermal manipulation produced the greatest changes in calcium signaling after stimulation.

In general, we found that vermal stimulation often resulted in stronger hippocampal modulation than simplex stimulation; in addition to stronger effects on cFos expression and postlight calcium signaling, vermal (lobule IV/V) stimulation produced stronger LFP changes and uniquely produced a postlight increase in correlated activity. Previous work examining coordinated changes in cFos expression in trained animals after performing a navigation task also suggested a particularly unique association between CA1 and lobule IV/V (Babayan et al., 2017).

Our current findings additionally provide important insight into previous experiments conducted using a mouse model of temporal lobe epilepsy (Krook-Magnuson et al., 2014), which used the same light parameters and targeted the same regions of the cerebellum as examined in our current work. In that previous study, on-demand optogenetic manipulation of the cerebellum, regardless of the location targeted, acutely inhibited spontaneous hippocampal seizures (an outcome that may be related to the acute decrease in activity at the time of light delivery, shown in Fig. 4*f*, and altered coordinated activity, shown in Fig. 5). Particularly relevant to this discussion, that study observed an additional unique benefit with vermal activation; vermal stimulation (but not simplex stimulation) also produced a lasting anti-seizure effect, which, though brief, substantially outlasted the duration of light delivery (Krook-Magnuson et al., 2014). In the context of our current work, this may be because of the larger postlight impact observed with vermal stimulation (e.g., on calcium event amplitudes and correlated activity).

Given the distinct yet overlapping influences of the vermis lobule IV/V and simplex on the hippocampus, there may be parallel (and to some extent converging) lines of cerebellar influence over the hippocampus. Of interest, our cFos results following either simplex or vermal (lobule IV/V) targeting indicated that dentate gyrus granule cells were not strongly impacted by our manipulations, at least so far as cFos is able to illustrate (see, e.g., X. Sun et al., 2020). This suggests a route of influence distinct from the classical trisynaptic pathway (van Strien et al., 2009; Y. Sun et al., 2014, 2019). However, our cFos data do not indicate that we had no effect on the dentate gyrus (indeed, we noted a slight increase in cFos expression in molecular layer interneurons in the dentate gyrus), nor does it indicate that no region of the cerebellum may influence dentate gyrus granule cells. Indeed, a recent tracing study, in which rabies was injected into the dentate gyrus of mice, found evidence for (multisynaptic) connectivity between the dentate gyrus and other regions of the cerebellum, including crus I and lobule VI) (Watson et al., 2019). This further strengthens the view that there may be multiple routes by which distinct regions of the cerebellum can provide their own influence on hippocampal networks (Rondi-Reig et al., 2014; Diedrichsen et al., 2019; Krook-Magnuson, 2020).

Recent evidence suggests that there is no direct pathway from the cerebellum to the hippocampus (Bohne et al., 2019; Watson et al., 2019; Krook-Magnuson, 2020), and determining which anatomic pathways functionally connect the two structures is an area of active investigation. Purkinje cells typically project to the cerebellar nuclei. Cerebellar nuclei project to a number of thalamic nuclei (Haroian et al., 1981; Fujita et al., 2020), and it can be tempting to speculate on potential pathways to the hippocampus from these targets. Thalamic nuclei may have indirect effects

on CA1 via retrosplenial (Werf et al., 2002), anterior cingulate (Rajasethupathy et al., 2015), or subicular (Y. Sun et al., 2019) relays. However, there are several extrathalamic ways for the cerebellum to influence the hippocampus. Vestibular nuclei, and the vestibular system more broadly, may also influence spatial processing (Hitier et al., 2014). Additionally, Purkinje cells are reported to have direct (bypassing the cerebellar nuclei) projections to the locus ceruleus (Schwarz et al., 2015), which in turn can impact CA1 place cells (Kaufman et al., 2020). The reticular formation, including the medial, magnocellular aspect, receives cerebellar nuclear input (Faull and Carman, 1978; Fujita et al., 2020) and has a long-standing history of modulating hippocampal LFP (N. McNaughton and Sedgwick, 1978; Vertes, 1980; N. McNaughton et al., 1986; Munn et al., 2015). The nucleus incertus has both indirect (via the septum) (Goto et al., 2001; Olucha-Bordonau et al., 2003) and direct (Szőnyi et al., 2019) projections to the hippocampus, specifically targeting CA1 neurons in the stratum oriens (in line with our cFos results). Similarly, the septum and supramammilary nucleus may receive direct cerebellar projections (Heath et al., 1978; Fujita et al., 2020) and in turn project to the hippocampus (Soussi et al., 2010; Unal et al., 2015; Hashimotodani et al., 2018; Watson et al., 2019). Timed transynaptic tracing studies suggest a disynaptic pathway between the hippocampal formation and cerebellar nuclei, fitting with these pathways (Watson et al., 2019). Additional possible pathways exist; and as noted above, there may be several routes by which the cerebellum, and different aspects of the cerebellum, influence the hippocampus. Determining which of these potential pathways mediates functional connectivity, and what physiological function each serves, will be an important area of future investigations.

Our data demonstrate robust and specific influences of optogenetic cerebellar excitation on hippocampal function at the cellular, population, and behavioral levels. Moreover, our findings reveal that two different sites of cerebellar modulation, the simplex and lobule IV/V of the vermis, exhibit broadly similar effects on gross hippocampal function, yet differ with respect to duration and strength of modulation. Our findings provide strong support for the cerebellum not being only a motor-related structure, but also having influence on more cognitive functions (Popa et al., 2014; Diedrichsen et al., 2019; Shipman and Green, 2019). Notably, work examining the "cognitive cerebellum" often focuses on the lateral hemispheres of the cerebellum, in part because of expansion in evolution and connectivity with neocortex (Schmahmann, 2019). Our work clearly illustrates that the cerebellar vermis and simplex can be powerful modulators of hippocampal dynamics and function, and should therefore not be overlooked when considering cerebellar regions which may contribute to cognitive functions.

References

Aravanis AM, Wang LP, Zhang F, Meltzer LA, Mogri MZ, Schneider MB, Deisseroth K (2007) An optical neural interface: in vivo control of rodent motor cortex with integrated fiberoptic and optogenetic technology. J Neural Eng 4:S143–S156.

Argyropoulos GP, van Dun K, Adamaszek M, Leggio M, Manto M, Masciullo M, Molinari M, Stoodley CJ, Van Overwalle F, Ivry RB, Schmahmann JD (2020) The cerebellar cognitive affective/Schmahmann syndrome: a task force paper. Cerebellum 19:102–125.

Babayan BM, Watilliaux A, Viejo G, Paradis AL, Girard B, Rondi-Reig L (2017) A hippocampo-cerebellar centred network for the learning and execution of sequence-based navigation. Sci Rep 7:17812.

Badura A, Verpeut JL, Metzger JW, Pereira TD, Pisano TJ, Deverett B, Bakshinskaya DE, Wang S (2018) Normal cognitive and social development require posterior cerebellar activity. eLife 7:e36401.

Balderas I, Rodriguez-Ortiz CJ, Salgado-Tonda P, Chavez-Hurtado J, McGaugh JL, Bermudez-Rattoni F (2008) The consolidation of object and context recognition memory involve different regions of the temporal lobe. Learn Mem 15:618–624.

Barry C, Burgess N (2014) Neural mechanisms of self-location. Curr Biol 24: R330–R339.

Bohne P, Schwarz MK, Herlitze S, Mark MD (2019) A new projection from the deep cerebellar nuclei to the hippocampus via the ventrolateral and laterodorsal thalamus in mice. Front Neural Circuits 13:51.

Broadbent NJ, Squire LR, Clark RE (2004) Spatial memory, recognition memory, and the hippocampus. Proc Natl Acad Sci USA 101:14515–14520.

Burke SN, Maurer AP, Nematollahi S, Uprety AR, Wallace JL, Barnes CA (2011) The influence of objects on place field expression and size in distal hippocampal CA1. Hippocampus 21:783–801.

Buzsáki G (1986) Hippocampal sharp waves: their origin and significance. Brain Res 398:242–252.

Cai DJ, Aharoni D, Shuman T, Shobe J, Biane J, Song W, Wei B, Veshkini M, La-Vu M, Lou J, Flores SE, Kim I, Sano Y, Zhou M, Baumgaertel K, Lavi A, Kamata M, Tuszynski M, Mayford M, Golshani P, et al. (2016) A shared neural ensemble links distinct contextual memories encoded close in time. Nature 534:115–118.

Carta I, Chen CH, Schott AL, Dorizan S, Khodakhah K (2019) Cerebellar modulation of the reward circuitry and social behavior. Science 363: eaav0581.

Chen TW, Wardill TJ, Sun Y, Pulver SR, Renninger SL, Baohan A, Schreiter ER, Kerr RA, Orger MB, Jayaraman V, Looger LL, Svoboda K, Kim DS (2013) Ultrasensitive fluorescent proteins for imaging neuronal activity. Nature 499:295–300.

Choe KY, Sanchez CF, Harris NG, Otis TS, Mathews PJ (2018) Optogenetic fMRI and electrophysiological identification of region-specific connectivity between the cerebellar cortex and forebrain. Neuroimage 173:370–383.

Christenson Wick Z, Tetzlaff MR, Krook-Magnuson E (2019) Novel long-range inhibitory nNOS-expressing hippocampal cells. Elife 8:e46816.

Chrobak JJ, Buzsáki G (1996) High-frequency oscillations in the output networks of the hippocampal-entorhinal axis of the freely behaving rat. J Neurosci 16:3056–3066.

Ciernia AV, Wood M (2014) Examining object location and object recognition memory in mice. J Curr Protoc Neurosci 69:8.31.1–38.31.17.

Colombel C, Lalonde R, Caston J (2004) The effects of unilateral removal of the cerebellar hemispheres on spatial learning and memory in rats. Brain Res 1004:108–115.

Danielson NB, Zaremba JD, Kaifosh P, Bowler J, Ladow M, Losonczy A (2016) Sublayer-specific coding dynamics during spatial navigation and learning in hippocampal area CA1. Neuron 91:652–665.

Deshmukh SS, Knierim JJ (2011) Representation of non-spatial and spatial information in the lateral entorhinal cortex. Front Behav Neurosci 5:69.

Deshmukh SS, Knierim JJ (2013) Influence of local objects on hippocampal representations: landmark vectors and memory. Hippocampus 23:253–267.

Diedrichsen J, King M, Hernandez-Castillo C, Sereno M, Ivry RB (2019) Universal transform or multiple functionality? Understanding the contribution of the human cerebellum across task domains. Neuron 102:918–928.

Eichenbaum H, Cohen NJ (2014) Can we reconcile the declarative memory and spatial navigation views on hippocampal function? Neuron 83:764–770.

Faull RL, Carman JB (1978) The cerebellofugal projections in the brachium conjunctivum of the rat: I. The contralateral ascending pathway. J Comp Neurol 178:495–517.

Flavell SW, Greenberg ME (2008) Signaling mechanisms linking neuronal activity to gene expression and plasticity of the nervous system. Annu Rev Neurosci 31:563–590.

Fujita H, Kodama T, Lac SD (2020) Modular output circuits of the fastigial nucleus mediate diverse motor and nonmotor functions of the cerebellar vermis. Elife 9:e58613.

Geiller T, Fattahi M, Choi JS, Royer S (2017) Place cells are more strongly tied to landmarks in deep than in superficial CA1. Nat Commun 8:14531.

Gornati SV, Schäfer CB, Rooda O, Nigg AL, Zeeuw CI, Hoebeek FE (2018) Differentiating cerebellar impact on thalamic nuclei. Cell Rep 23:2690–2704.

Goto M, Swanson LW, Canteras NS (2001) Connections of the nucleus incertus. J Comp Neurol 438:86–122.

Haettig J, Stefanko DP, Multani ML, Figueroa DX, McQuown SC, Wood MA (2011) HDAC inhibition modulates hippocampus-dependent long-term memory for object location in a CBP-dependent manner. Learn Mem 18:71–79.

Haroian AJ, Massopust LC, Young PA (1981) Cerebellothalamic projections in the rat: an autoradiographic and degeneration study. J Comp Neurol 197:217–236.

Hartley T, Lever C, Burgess N, O'Keefe J (2014) Space in the brain: how the hippocampal formation supports spatial cognition. Philos Trans R Soc Lond B Biol Sci 369:20120510.

Hashimotodani Y, Karube F, Yanagawa Y, Fujiyama F, Kano M (2018) Supramammillary nucleus afferents to the dentate gyrus co-release glutamate and GABA and potentiate granule cell output. Cell Rep 25:2704–2715.e4.

Heath RG, Dempesy CW, Fontana CJ, Myers WA (1978) Cerebellar stimulation: effects on septal region, hippocampus, and amygdala of cats and rats. Biol Psychiatry 13:501–529.

Hijazi S, Heistek TS, Scheltens P, Neumann U, Shimshek DR, Mansvelder HD, Smit AB, van Kesteren RE (2019) Early restoration of parvalbumin interneuron activity prevents memory loss and network hyperexcitability in a mouse model of Alzheimer's disease. Mol Psychiatry. Advance online publication. Retrieved August 20, 2019. doi: 10.1038/s41380-019-0483-4.

Hilber P, Jouen F, Delhaye-Bouchaud N, Mariani J, Caston J (1998) Differential roles of cerebellar cortex and deep cerebellar nuclei in learning and retention of a spatial task: studies in intact and cerebellectomized Lurcher mutant mice. Behav Genet 28:299–308.

Hippenmeyer S, Vrieseling E, Sigrist M, Portmann T, Laengle C, Ladle DR, Arber S (2005) A developmental switch in the response of DRG neurons to ETS transcription factor signaling. PLoS Biol 3:e159.

Hitier M, Besnard S, Smith PF (2014) Vestibular pathways involved in cognition. Frontiers Integr Neurosci 8:59.

Hochreiter S, Schmidhuber J (1997) Long short-term memory. Neural Comput 9:1735–1780.

Hoffmann LC, Berry SD (2009) Cerebellar theta oscillations are synchronized during hippocampal theta-contingent trace conditioning. Proc Natl Acad Sci USA 106:21371–21376.

Igarashi KM, Lu L, Colgin LL, Moser MB, Moser EI (2014) Coordination of entorhinal–hippocampal ensemble activity during associative learning. Nature 510:143–147.

Jarsky T, Mady R, Kennedy B, Spruston N (2008) Distribution of bursting neurons in the CA1 region and the subiculum of the rat hippocampus. J Comp Neurol 506:535–547.

Joyal CC, Meyer C, Jacquart G, Mahler P, Caston J, Lalonde R (1996) Effects of midline and lateral cerebellar lesions on motor coordination and spatial orientation. Brain Res 739:1–11.

Joyal CC, Strazielle C, Lalonde R (2001) Effects of dentate nucleus lesions on spatial and postural sensorimotor learning in rats. Behav Brain Res 122:131–137.

Kaufman AM, Geiller T, Losonczy A (2020) A role for the locus coeruleus in hippocampal CA1 place cell reorganization during spatial reward learning. Neuron 105:1018–1026.e4.

Kim HK, Gschwind T, Nguyen TM, Bui AD, Felong S, Ampig K, Suh D, Ciernia AV, Wood MA, Soltesz I (2020) Optogenetic intervention of seizures improves spatial memory in a mouse model of chronic temporal lobe epilepsy. Epilepsia 61:561–571.

King M, Hernandez-Castillo CR, Poldrack RA, Ivry RB, Diedrichsen J (2019) Functional boundaries in the human cerebellum revealed by a multi-domain task battery. Nat Neurosci 22:1371–1378.

Knierim JJ, Neunuebel JP, Deshmukh SS (2014) Functional correlates of the lateral and medial entorhinal cortex: objects, path integration and local–global reference frames. Philos Trans R Soc Lond B Biol Sci 369:20130369.

Komorowski RW, Manns JR, Eichenbaum H (2009) Robust conjunctive item-place coding by hippocampal neurons parallels learning what happens where. J Neurosci 29:9918–9929.

Kravitz DJ, Saleem KS, Baker CI, Mishkin M (2011) A new neural framework for visuospatial processing. Nat Rev Neurosci 12:217–230.

Krook-Magnuson E (2020) From point A to point B, and what it means for epilepsy. Epilepsy Curr 20:51–53.

Krook-Magnuson E, Szabo GG, Armstrong C, Oijala M, Soltesz I (2014) Cerebellar directed optogenetic intervention inhibits spontaneous hippocampal seizures in a mouse model of temporal lobe epilepsy. eNeuro 1: ENEURO.0005-14.2014.

LeCun Y, Bengio Y, Hinton G (2015) Deep learning. Nature 521:436–444.

Lefort JM, Vincent J, Tallot L, Jarlier F, Zeeuw CI, Rondi-Reig L, Rochefort C (2019) Impaired cerebellar Purkinje cell potentiation generates unstable spatial map orientation and inaccurate navigation. Nat Commun 10:2251.

Leggio MG, Molinari M, Neri P, Graziano A, Mandolesi L, Petrosini L (2000) Representation of actions in rats: the role of cerebellum in learning spatial performances by observation. Proc Natl Acad Sci USA 97:2320–2325.

Leggio MG, Neri P, Graziano A, Mandolesi L, Molinari M, Petrosini L (1999) Cerebellar contribution to spatial event processing: characterization of procedural learning. Exp Brain Res 127:1–11.

Leong AT, Gu Y, Chan YS, Zheng H, Dong CM, Chan RW, Wang X, Liu Y, Tan LH, Wu EX (2019) Optogenetic fMRI interrogation of brain-wide central vestibular pathways. Proc Natl Acad Sci USA 116:10122–10129.

Locke TM, Soden ME, Miller SM, Hunker A, Knakal C, Licholai JA, Dhillon KS, Keene CD, Zweifel LS, Carlson ES (2018) Dopamine D1 receptor-positive neurons in the lateral nucleus of the cerebellum contribute to cognitive behavior. Biol Psychiatry 84:401–412.

Lu J, Li C, Singh-Alvarado J, Zhou Z, Fröhlich F, Mooney R, Wang F (2018) MIN1PIPE: a Miniscope 1-photon-based calcium imaging signal extraction pipeline. Cell Rep 23:3673–3684.

Lucas B, Kanade T (1981) An iterative image registration technique with an application to stereo vision. In: Proceedings of the 1981 DARPA Image Understanding Workshop, Vol 2, pp 674–679. San Francisco, CA: Morgan Kaufmann Publishers Inc.

Madisen L, Mao T, Koch H, Zhuo J, Berenyi A, Fujisawa S, Hsu YW, Garcia AJ, Gu X, Zanella S, Kidney J, Gu H, Mao Y, Hooks BM, Boyden ES, Buzsáki G, Ramirez JM, Jones AR, Svoboda K, Han X, et al. (2012) A toolbox of Cre-dependent optogenetic transgenic mice for light-induced activation and silencing. Nat Neurosci 15:793–802.

Mandolesi L, Leggio MG, Spirito F, Federico F, Petrosini L (2007) Is the cerebellum involved in the visuo-locomotor associative learning? Behav Brain Res 184:47–56.

Manns JR, Eichenbaum H (2009) A cognitive map for object memory in the hippocampus. Learn Mem Cold Mem 16:616–624.

Masurkar AV, Srinivas KV, Brann DH, Warren R, Lowes DC, Siegelbaum SA (2017) Medial and lateral entorhinal cortex differentially excite deep versus superficial CA1 pyramidal neurons. Cell Rep 18:148–160.

McAfee SS, Liu Y, Sillitoe RV, Heck DH (2019) Cerebellar lobulus simplex and crus I differentially represent phase and phase difference of prefrontal cortical and hippocampal oscillations. Cell Rep 27:2328–2334.e3.

McNaughton BL, Battaglia FP, Jensen O, Moser EI, Moser MB (2006) Path integration and the neural basis of the "cognitive map." Nat Rev Neurosci 7:663–678.

McNaughton N, Sedgwick EM (1978) Reticular stimulation and hippocampal theta rhythm in rats: effects of drugs. Neuroscience 3:629–632.

McNaughton N, Richardson J, Gore C (1986) Reticular elicitation of hippocampal slow waves: common effects of some anxiolytic drugs. Neuroscience 19:899–903.

Minatohara K, Akiyoshi M, Okuno H (2016) Role of immediate-early genes in synaptic plasticity and neuronal ensembles underlying the memory trace. Front Mol Neurosci 8:78.

Mitra P, Bokil H (2008) Observed brain dynamics. Oxford: Oxford UP.

Mizuseki K, Diba K, Pastalkova E, Buzsáki G (2011) Hippocampal CA1 pyramidal cells form functionally distinct sublayers. Nat Neurosci 14:1174–1181.

Morgan JI, Curran T (1986) Role of ion flux in the control of c-fos expression. Nature 322:552–555.

Moulton EA, Elman I, Becerra LR, Goldstein RZ, Borsook D (2014) The cerebellum and addiction: insights gained from neuroimaging research. Addict Biol 19:317–331.

Mumby DG, Gaskin S, Glenn MJ, Schramek TE, Lehmann H (2002) Hippocampal damage and exploratory preferences in rats: memory for objects, places, and contexts. Learn Mem 9:49–57.

Munn RG, Tyree SM, McNaughton N, Bilkey DK (2015) The frequency of hippocampal theta rhythm is modulated on a circadian period and is entrained by food availability. Front Behav Neurosci 9:61.

O'Keefe J, Nadel L (1978) The hippocampus as a cognitive map. Oxford: Clarendon Press.

Olucha-Bordonau FE, Teruel V, Barcia-González J, Ruiz-Torner A, Valverde-Navarro AA, Martínez-Soriano F (2003) Cytoarchitecture and efferent projections of the nucleus incertus of the rat: cytoarchitectonics and efferents of the nucleus incertus. J Comp Neurol 464:62–97.

Pennington ZT, Dong Z, Feng Y, Vetere LM, Page-Harley L, Shuman T, Cai DJ (2019) ezTrack: an open-source video analysis pipeline for the investigation of animal behavior. Sci Rep 9:19979.

Perona P, Malik J (1990) Scale-space and edge detection using anisotropic diffusion. IEEE Trans Pattern Anal Machine Intell 12:629–639.

Peter S, Brinke MM, Stedehouder J, Reinelt CM, Wu B, Zhou H, Zhou K, Boele HJ, Kushner SA, Lee MG, Schmeisser MJ, Boeckers TM, Schonewille M, Hoebeek FE, Zeeuw CI (2016) Dysfunctional cerebellar Purkinje cells contribute to autism-like behaviour in Shank2-deficient mice. Nat Commun 7:12627.

Petrosini L, Molinari M, Dell'Anna ME (1996) Cerebellar contribution to spatial event processing: Morris Water Maze and T-maze. Eur J Neurosci 8:1882–1896.

Pnevmatikakis EA, Soudry D, Gao Y, Machado TA, Merel J, Pfau D, Reardon T, Mu Y, Lacefield C, Yang W, Ahrens M, Bruno R, Jessell TM, Peterka DS, Yuste R, Paninski L (2016) Simultaneous denoising, deconvolution, and demixing of calcium imaging data. Neuron 89:285–299.

Popa LS, Hewitt AL, Ebner TJ (2014) The cerebellum for jocks and nerds alike. Front Syst Neurosci 8:113.

Rajasethupathy P, Sankaran S, Marshel JH, Kim CK, Ferenczi E, Lee S, Berndt A, Ramakrishnan C, Jaffe A, Lo M, Liston C, Deisseroth K (2015) Projections from neocortex mediate top-down control of memory retrieval. Nature 526:653–659.

Redish A (1999) Beyond the cognitive map: from place cells to episodic memory. Cambridge, MA: Massachusetts Institute of Technology.

Rochefort C, Arabo A, André M, Poucet B, Save E, Rondi-Reig L (2011) Cerebellum shapes hippocampal spatial code. Science 334:385–389.

Rochefort C, Lefort JM, Rondi-Reig L (2013) The cerebellum: a new key structure in the navigation system. Front Neural Circuits 7:35.

Rondi-Reig L, Paradis AL, Lefort JM, Babayan BM, Tobin C (2014) How the cerebellum may monitor sensory information for spatial representation. Front Syst Neurosci 8:205.

Sabariego M, Schönwald A, Boublil BL, Zimmerman DT, Ahmadi S, Gonzalez N, Leibold C, Clark RE, Leutgeb JK, Leutgeb S (2019) Time cells in the hippocampus are neither dependent on medial entorhinal cortex inputs nor necessary for spatial working memory. Neuron 102:1235–1248.e5.

Savelli F, Knierim JJ (2019) Origin and role of path integration in the cognitive representations of the hippocampus: computational insights into open questions. J Exp Biol 222:jeb188912.

Schindelin J, Arganda-Carreras I, Frise E, Kaynig V, Longair M, Pietzsch T, Preibisch S, Rueden C, Saalfeld S, Schmid B, Tinevez JY, White DJ, Hartenstein V, Eliceiri K, Tomancak P, Cardona A (2012) Fiji: an open-source platform for biological-image analysis. Nat Methods 9:676–682.

Schmahmann JD (1996) From movement to thought: anatomic substrates of the cerebellar contribution to cognitive processing. Hum Brain Mapp 4:174–198.

Schmahmann JD (2019) The cerebellum and cognition. Neurosci Lett 688:62–75.

Schwarz LA, Miyamichi K, Gao XJ, Beier KT, Weissbourd B, DeLoach KE, Ren J, Ibanes S, Malenka RC, Kremer EJ, Luo L (2015) Viral-genetic tracing of the input-output organization of a central noradrenaline circuit. Nature 524:88–92.

Serra J, Vincent L (1992) An overview of morphological filtering. Circuits Syst Signal Process 11:47–108.

Shi J, Tomasi C (1994) Good features to track. Proceedings of the IEEE Conference on Computer Vision and Pattern Recognition, Seattle.

Shipman ML, Green JT (2019) Cerebellum and cognition: does the rodent cerebellum participate in cognitive functions? Neurobiol Learn Mem 13:106996.

Shuman T, Aharoni D, Cai DJ, Lee CR, Chavlis S, Page-Harley L, Vetere LM, Feng Y, Yang CY, Mollinedo-Gajate I, Chen L, Pennington ZT, Taxidis J, Flores SE, Cheng K, Javaherian M, Kaba CC, Rao N, La-Vu M, Pandi I, et al. (2020) Breakdown of spatial coding and interneuron synchronization in epileptic mice. Nat Neurosci 23:229–210.

Skaggs WE, McNaughton BL, Gothard KM, Markus EJ (1993) An information-theoretic approach to deciphering the hippocampal code. In: Neural information processing systems (Hanson S, Cowan JD, Giles CL eds), 1030–1037. San Mateo, CA: Kaufman.

Sneider JT, Chrobak JJ, Quirk MC, Oler JA, Markus EJ (2006) Differential behavioral state-dependence in the burst properties of CA3 and CA1 neurons. Neuroscience 141:1665–1677.

Soltesz I, Losonczy A (2018) CA1 pyramidal cell diversity enabling parallel information processing in the hippocampus. Nat Neurosci 21:484–493.

Soussi R, Zhang N, Tahtakran S, Houser CR, Esclapez M (2010) Heterogeneity of the supramammillary-hippocampal pathways: evidence for a unique GABAergic neurotransmitter phenotype and regional differences: GABAergic and glutamatergic supramammillary-hippocampal pathways. Eur J Neurosci 32:771–785.

Strange BA, Witter MP, Lein ES, Moser EI (2014) Functional organization of the hippocampal longitudinal axis. Nat Rev Neurosci 15:655–669.

Strick PL, Dum RP, Fiez JA (2009) Cerebellum and nonmotor function. Annu Rev Neurosci 32:413–434.

Sun X, Bernstein MJ, Meng M, Rao S, Sørensen AT, Yao L, Zhang X, Anikeeva PO, Lin Y (2020) Functionally distinct neuronal ensembles within the memory engram. Cell 181:410–423.e17.

Sun Y, Nguyen AQ, Nguyen JP, Le L, Saur D, Choi J, Callaway EM, Xu X (2014) Cell-type-specific circuit connectivity of hippocampal CA1 revealed through Cre-dependent rabies tracing. Cell Rep 7:269–280.

Sun Y, Jin S, Lin X, Chen L, Qiao X, Jiang L, Zhou P, Johnston KG, Golshani P, Nie Q, Holmes TC, Nitz DA, Xu X, (2019) CA1-projecting subiculum neurons facilitate object–place learning. Nat Neurosci 22:1857–1870.

Szőnyi A, Sos KE, Nyilas R, Schlingloff D, Domonkos A, Takács VT, Pósfai B, Hegedüs P, Priestley JB, Gundlach AL, Gulyás AI, Varga V, Losonczy A, Freund TF, Nyiri G (2019) Brainstem nucleus incertus controls contextual memory formation. Science 364:eaaw0445.

Tsai PT, Hull C, Chu Y, Greene-Colozzi E, Sadowski AR, Leech JM, Steinberg J, Crawley JN, Regehr WG, Sahin M (2012) Autistic-like behaviour and cerebellar dysfunction in Purkinje cell Tsc1 mutant mice. Nature 488:647–651.

Unal G, Joshi A, Viney TJ, Kis V, Somogyi P (2015) Synaptic targets of medial septal projections in the hippocampus and extrahippocampal cortices of the mouse. J Neurosci 35:15812–15826.

Valero M, de la Prida L (2018) The hippocampus in depth: a sublayer-specific perspective of entorhinal–hippocampal function. Curr Opin Neurobiol 52:107–114.

Valero M, Cid E, Averkin RG, Aguilar J, Sanchez-Aguilera A, Viney TJ, Gomez-Dominguez D, Bellistri E, de la Prida L (2015) Determinants of different deep and superficial CA1 pyramidal cell dynamics during sharp-wave ripples. Nat Neurosci 18:1281–1290.

van Strien NM, Cappaert NL, Witter MP (2009) The anatomy of memory: an interactive overview of the parahippocampal-hippocampal network. Nat Rev Neurosci 10:272–282.

Vercauteren T, Pennec X, Perchant A, Ayache N (2009) Diffeomorphic demons: efficient non-parametric image registration. Neuroimage 45: S61–S72.

Vertes RP (1980) Brain stem activation of the hippocampus: a role for the magnocellular reticular formation and the MLF. Electroencephalogr Clin Neurophysiol 50:48–58.

Wagner MJ, Kim TH, Savall J, Schnitzer MJ, Luo L (2017) Cerebellar granule cells encode the expectation of reward. Nature 544:96–100.

Wang C, Chen X, Lee H, Deshmukh SS, Yoganarasimha D, Savelli F, Knierim JJ (2018a) Egocentric coding of external items in the lateral entorhinal cortex. Science 362:945–949.

Wang Y, Liang J, Chen L, Shen Y, Zhao J, Xu C, Wu X, Cheng H, Ying X, Guo Y, Wang S, Zhou Y, Wang Y, Chen Z (2018b) Pharmaco-genetic

therapeutics targeting parvalbumin neurons attenuate temporal lobe epilepsy. Neurobiol Dis 117:149–160.

Watson T, Obiang P, Torres-Herraez A, Watilliaux A, Coulon P, Rochefort C, Rondi-Reig L (2019) Anatomical and physiological foundations of cerebello-hippocampal interaction. eLife 8:e41896.

Werf YD, der Witter MP, Groenewegen HJ (2002) The intralaminar and midline nuclei of the thalamus: anatomical and functional evidence for participation in processes of arousal and awareness. Brain Res Brain Res Rev 39:107–140.

Wikgren J, Nokia MS, Penttonen M (2010) Hippocampo–cerebellar theta band phase synchrony in rabbits. Neuroscience 165:1538–1545.

Winters BD, Bussey TJ (2005) Transient inactivation of perirhinal cortex disrupts encoding, retrieval, and consolidation of object recognition memory. J Neurosci 25:52–61.

Winters BD, Forwood SE, Cowell RA, Saksida LM, Bussey TJ (2004) Double dissociation between the effects of peri-postrhinal cortex and hippocampal lesions on tests of object recognition and spatial memory: heterogeneity of function within the temporal lobe. J Neurosci 24:5901–5908.

Yu W, Krook-Magnuson E (2015) Cognitive collaborations: bidirectional functional connectivity between the cerebellum and the hippocampus. Front Syst Neurosci 9:177.

Zeidler Z, Brandt-Fontaine M, Leintz C, Krook-Magnuson C, Netoff T, Krook-Magnuson E (2018) Targeting the mouse ventral hippocampus in the intrahippocampal kainic acid model of temporal lobe epilepsy. eNeuro 5:ENEURO.0158-18.2018.

Zhang X, Ng AH, Tanner JA, Wu W, Copeland NG, Jenkins NA, Huang J (2004) Highly restricted expression of Cre recombinase in cerebellar Purkinje cells. Genesis 40:45–51.

Zhou P, Resendez SL, Rodriguez-Romaguera J, Jimenez JC, Neufeld SQ, Giovannucci A, Friedrich J, Pnevmatikakis EA, Stuber GD, Hen R, Kheirbek MA, Sabatini BL, Kass RE, Paninski L (2018) Efficient and accurate extraction of in vivo calcium signals from microendoscopic video data. eLife 7:e28728.